Distinguishing Protein and Gene Delivery Enables Characterization and Bioengineering of Extracellular Vesicle-Adeno-Associated Virus Vectors

Jonathan D. Boucher[1,2,3], Devin M. Stranford[1,3,4], Hailey I. Edelstein[1,3,4], Danielle Tullman-Ercek[1-3,5], Neha P. Kamat[3,5,6], Joshua N. Leonard[1-5,7*]

[1] Department of Chemical and Biological Engineering, Northwestern University, Evanston, Illinois 60208, United States

[2] Interdisciplinary Biological Sciences Program, Northwestern University, Evanston, Illinois 60208, United States

[3] Center for Synthetic Biology, Northwestern University, Evanston, Illinois 60208, United States

[4] Syenex Inc, Evanston, Illinois 60201, United States

[5] Chemistry of Life Processes Institute, Northwestern University, Evanston, Illinois 60208, United States

[6] Department of Biomedical Engineering, Northwestern University, Evanston, IL, 60208 USA

[7] Member, Robert H. Lurie Comprehensive Cancer Center, Northwestern University, Evanston, Illinois 60208, United States

Contact Information

*Corresponding author: Joshua N. Leonard, j-leonard@northwestern.edu

ABSTRACT

Adeno-associated virus (AAV) gene therapies have achieved clinical success, with multiple products reaching regulatory approval. Encapsulation of AAV vectors within engineered extracellular vesicles (EVs) is an emerging strategy which could help overcome challenges including pre-existing anti-capsid immunity and the need for controlling targeting and tropism. To guide the development of EV-AAV technologies, we developed an assay for quantifying and controlling for the contribution of pseudotransduction to evaluations of EV-AAV-mediated gene delivery. We developed an AAV vector that switches its transgene output from one reporter to another when acted upon by Cre recombinase expressed in a recipient cell. Using this platform, we investigated EV-AAV transduction as a function of various engineered EV surface modifications. For actively endocytic cells (HEK293FTs), modifications that enhance EV uptake and membrane fusion influence protein delivery but not gene delivery. Conversely, in less endocytic Jurkat T cells, modifications enhancing EV uptake improved both protein and gene delivery. These conclusions held across multiple AAV serotypes. Our results resolve apparent conflicts in prior reports and suggest that effects of enhancing uptake and membrane fusion of EV-AAV vectors are recipient cell type specific. The methods developed here unambiguously dissect EV-AAV transduction mechanisms and can guide future bioengineering of EV-AAV vectors.

INTRODUCTION

Adeno-associated virus (AAV) gene therapies are poised to revolutionize the treatment of genetic diseases. Over the last decade, at least seven AAV-based gene therapies have been approved by the US Food and Drug Administration, with hundreds of clinical trials ongoing.[1] Current efforts focus on challenges such as evading preexisting humoral immunity[2], and reducing off-target tissue transduction[3], which both necessitate higher vector doses that are associated with adverse effects[4,5]. One potential strategy for addressing these needs is encapsulation of AAV within engineered extracellular vesicles (EVs).

EVs are nanoscale, membrane-bound particles secreted by all cells and include exosomes, microvesicles, and particles such as apoptotic bodies.[6] Exosomes are formed through the invagination of endosomal compartments, resulting in multivesicular bodies that fuse with the plasma membrane to release exosomes into the extracellular space. These vesicles protect their cargo—cytoplasmic RNA, proteins, and

51 other biomolecules—from degradation by nucleases and proteases.[7] Microvesicles bud from the cell
52 surface and encapsulate a distinct set of biomolecules.[6] When recipient cells take up EVs, some cargo
53 molecules can be released into the cytoplasm to impact cell state.[8,9] Because EVs mediate intercellular
54 communication, exhibit lower toxicity and immunogenicity than synthetic delivery vehicles, and have longer
55 circulation times *in vivo*, they are attractive candidates for therapeutic cargo delivery.[10-12]

56 An interesting observation is that when AAV particles are assembled in producer cells, secreted
57 EVs can incorporate AAV particles capable of conferring gene expression in recipient cells, and such EV-
58 AAV vehicles have distinct properties that are useful for gene delivery.[13] EV-AAVs can mediate gene
59 delivery to the mouse brain, even when using serotypes not generally able to cross the blood-brain barrier.[14]
60 EV-AAV1 and EV-AAV9 outperformed their free AAV (standard, non-enveloped AAV particle) counterparts
61 in transduction of cochlear hair cells in explant cultures.[15] EV-AAV1 encoding *Lhfpl5,* a protein required for
62 mechanotransduction in outer and inner hair cells and for which loss leads to profound deafness, improved
63 hearing and movement abnormalities in *Lhfpl5*$^{-/-}$ mice.[15] Upon intravitreal injection, EV-AAV2 outperformed
64 free AAV2 in retinal transduction via delivery of GFP, increasing transduction to cell types that are
65 transduced by free AAV2 as well as increasing the extent of transduction across different regions of the
66 retina.[16] EV-AAV8 encoding hF.IX enhanced correction of hemophilia B phenotypes compared to standard
67 AAV8 vectors in C57BL/6 *F9−/−* mice, demonstrating enhanced liver targeting after intravenous injection.[17]
68 Both standard AAV8 and EV-AAV8 can transduce a variety of immune cell populations, including CD4^{+} T
69 cells, CD8^{+} T cells, B cells, macrophages, and dendritic cells after systemic delivery in mice.[18] EV-AAV8
70 can mediate the expression of human interleukin-2 receptor alpha chain (IL-2Rα) in multiple lymphocyte
71 populations, suggesting that EV-AAVs could be utilized for *in vivo* cell engineering.[18] In a lung cancer
72 xenograft mouse model, local injection of EV-AAV6 was much more potent in transducing tumor cells
73 compared to free AAV6.[19] Upon intratracheal injection in C57BL/6 mice, EV-AAV6 enhanced transduction
74 of the lung compared to either free AAV6 or a mixture of free AAV6 and EVs, demonstrating that the
75 enhanced lung transduction by EV-AAV6 was attributable to the direct association of EVs and AAV6.[20] EV-
76 AAV9 delivering *SERCA2a* significantly improved cardiac function in a mouse model of myocardial
77 infarction compared to free AAV9.[21] In addition to improving transduction, EV-AAVs resist neutralization by
78 AAV specific antibodies, suggesting that encapsulation can help address needs for AAV vector

79 delivery.[14,17,19-25] Moreover, since EVs have been engineered to target specific cell types[26-29], it is possible
80 that such methods could target EV-AAVs as well.

81 Although EV-AAV vectors are promising, several key mechanistic questions are incompletely
82 understood. First, the functional consequences of surface-functionalizing EV-AAV vectors on recipient cell
83 binding and particle uptake are unclear. Second, reports conflict as to how increasing EV-endosomal fusion
84 modulates transduction by EV-AAV. An early study suggested that functionalizing EV-AAVs by incorporating
85 the low pH-activated fusogen vesicular stomatitis virus glycoprotein (VSV-G) on the EV surface can diminish
86 transduction of HEK293T and U87 glioma cells by AAV2, compared to EV-AAV2 lacking VSV-G.[30] This is
87 surprising as increasing uptake (via VSV-G binding to its receptor, low density lipoprotein receptor, LDL-
88 R[31]) and fusion-mediated entry of the AAV capsid into the cytosol may be expected to increase transduction.
89 While a possible explanation is that AAV2 requires processing in the endosome—capsid cleavage by the
90 endosomal cysteine proteases cathepsins B and L[32], autoproteolytic processing of the capsid at low
91 pH[33], and exposure of the VP1/2 N-terminal region exposing a phospholipase A2 domain that helps the
92 virion escape the endosome and traffic to the nucleus[34,35]—that mechanism is untested in EV-AAV delivery.
93 VSV-G display on EV-AAV2 showed no effect on gene delivery to several other glioma cell lines compared
94 to non-targeted EV-AAV2[30], suggesting the role of VSV-G may vary by recipient cell type. A related line of
95 evidence is that display of rabies virus glycoprotein (RVG) on the surface of EV-AAV9 increased
96 transduction of SH-SY5Y cells and gene delivery to the brain of mice compared to non-targeted EV-AAV9.[22]
97 RVG binds to the nicotinic acetylcholine receptor (nAChR), neural cell adhesion molecule (NCAM), p75
98 neurotrophin receptor, integrin β1, and transferrin receptor 1 (TfR1), promoting clathrin-mediated
99 endocytosis of the particle.[36] Much like VSV-G, upon encountering the low pH of the endosome, RVG
100 undergoes conformational changes that promote endosomal membrane fusion and escape.[37,38] Given the
101 similarity in mechanisms used by VSV-G and RVG, the differences in transduction when displayed on EV-
102 AAVs is surprising and may indicate recipient cell type and/or AAV serotype-specific effects. Thus, although
103 EV-AAV vectors are promising, successful bioengineering of such vectors would benefit from mechanistic
104 understanding of delivery mechanisms.

105 A key technical challenge when evaluating engineered EV-AAV-mediated delivery is distinguishing
106 delivery of protein originating from transgene expression in producer cells (i.e., “pseudotransduction”), from

107 gene delivery to and resulting transgene expression in recipient cells. This challenge is analogous to the
108 pseudotransduction observed with lentiviral and retroviral vectors, which are also enveloped and can
109 incorporate cytosolic proteins from producer cells.[39-42] In certain applications, pseudotransduction may be
110 useful, as demonstrated in dendritic cell–targeted lentiviral vectors for vaccination, in which incorporated
111 protein antigens are employed to train induced immune reactions.[43] However, in applications where
112 quantification of gene delivery or transduction is desired, pseudotransduction can inflate the rates of
113 transduction reported. Informed in part by prior observations that protein delivery can complicate evaluation
114 of EV-mediated mRNA delivery[44,45], we hypothesized that controlling for pseudotransduction may be
115 particularly crucial for measuring EV-AAV transduction because achieving comparable rates of transduction
116 typically requires higher numbers of particles for EV-AAV compared to lentiviral vectors. Thus,
117 distinguishing transduction from pseudotransduction (protein delivery) is critical for the engineering and
118 evaluation of EV-AAV vectors.

119 In this study, we developed and validated a quantitative assay for disambiguating
120 pseudotransduction from transduction by EV-AAVs and applied this method to investigate several biological
121 hypotheses that inform bioengineering. Our assay comprises a modified stoplight system, in which Cre
122 recombinase is expressed in recipient cells where it can modify an incoming engineered AAV vector to shift
123 its transgene expression from one fluorescent protein to another. Using this approach, pseudotransduction
124 (protein delivery) and transduction (gene delivery) can be measured separately. With this system, we
125 compared various EV surface functionalization strategies that drive uptake and/or membrane fusion with
126 recipient cells and determined how these engineering choices impact protein and gene delivery. Such
127 analysis revealed new insights about EV-AAV transduction that would otherwise be obscured by
128 pseudotransduction. Our assay enables generation and testing of new mechanistic hypotheses for studying
129 EV-AAV biology and bioengineering these vectors.

130

131 **METHODS**

132

133 ***General DNA assembly***

134 Plasmids were constructed using standard molecular biology techniques. Plasmid assembly was performed
135 via restriction enzyme cloning. Plasmids were transformed into TOP10 competent Escherichia coli (Thermo
136 Fisher) and grown at 37 °C. AAV vector (transfer) plasmids were transformed into NEB Stable competent
137 Escherichia coli (New England Biolabs C3040) and grown at 37 °C. Plasmid cloning was performed
138 primarily using standard restriction enzyme cloning with restriction enzymes (NEB), T4 DNA Ligase (NEB
139 M0202L), and Antarctic Phosphatase (NEB M0289L). Plasmids with pcDNA-based backbones were
140 transformed into chemically competent TOP10 *Escherichia coli* (Thermo Fisher C404010), and cells were
141 grown at 37°C. Plasmids with AAV transgene vector backbones were transformed into chemically
142 competent NEB Stable *Escherichia coli* (NEB C3040H), and cells were grown at 30°C.
143
144 ***Source vectors for DNA assembly***
145 The AAV transfer vector (pAAV-GFP SN), and helper plasmid (pHelper) were gifts from David Schaffer
146 (University of California, Berkeley). The LumiScarlet gene was PCR amplified from pcDNA3-LumiScarlet,
147 which was a gift from Huiwang Ai (Addgene plasmid # 126623 ; http://n2t.net/addgene:126623 ;
148 RRID:Addgene_126623)[46], and cloned into the pAAVGFP SN plasmid using AgeI and NotI. pOTTC1032 -
149 pAAV EF1a Nuc-flox(mCherry)-EGFP (pJB037) was a gift from Brandon Harvey (Addgene plasmid #
150 112677 ; http://n2t.net/addgene:112677 ; RRID:Addgene_112677).[47] Gene strings for the other Cre-
151 responsive vectors (pJB038 - No NLS and eGFP, pJB040 - NLS and mNeonGreen, and pJB041 No NLS
152 and mNeonGreen) were codon optimized and synthesized by ThermoFisher (GeneArt), then cloned into
153 the pOCTTC1032 plasmid using KpnI and EcoRI restriction enzymes. RepCap plasmids for AAV2
154 (pRep2Cap2) and AAV6 (pRep2Cap6) were gifts from the Vector Core at the University of Pennsylvania
155 (Penn Vector Core (RRID: SCR_022432)). pcDNA is plasmid pPD005 (Addgene plasmid # 138749 ;
156 http://n2t.net/addgene:138749 ; RRID:Addgene_138749).[48] psPAX2 and pMD2.G plasmids were gifted by
157 William Miller from Northwestern University. pHIE822 was created by introducing point mutations (K47Q,
158 R354A) in the VSV-G-encoding gene of pMD2.G using site-directed mutagenesis by PCR. pCMV-VSV-
159 G(P127D)-Myc (pJB042) was a gift from Wesley Sundquist (Addgene plasmid # 80055 ;
160 http://n2t.net/addgene:80055 ; RRID:Addgene_80055).[49] pHIE963 was created using standard restriction
161 enzyme cloning to insert a Cre recombinase gene into a third-generation lentiviral transfer vector provided

162 by Twist Bioscience (pTwist Lenti SFFV PuroR). The Cre recombinase gene was amplified by PCR from
163 pBS185 CMV-Cre, which was a gift from Brian Sauer (Addgene plasmid # 11916
164 ; http://n2t.net/addgene:11916 ; RRID:Addgene_11916).[50] The Ultra-HEK plasmid is a commercial product
165 made by Syenex. The plasmids used to produce Ultra-HEK lentiviral vectors are Syenex plasmids: SNX-
166 mNG-TV3, SNX-Gagpol, SNX-Rev, and SNX-VSV-G. A list of plasmids utilized in this study can be found
167 in **Supplementary Data 1**. Plasmid sequences can be found in **Supplementary Data 2**.
168
169 ***Plasmid preparation***
170 TOP10 or NEB Stable *E. coli* were grown overnight, shaking at 37°C or 30°C, respectively, in 50-100 mL of
171 LB media with the appropriate selective antibiotic. The next day, DNA was prepped using a ZymoPURE II
172 Plasmid Midiprep Kit (Zymo D4201) following the manufacturer's instructions. DNA purity and
173 concentrations for relevant experiments were measured with a NanoDrop 2000 (Thermo Fisher Scientific).
174
175 ***Cell culture***
176 FreeStyle 293-F cells (Gibco R79007) cells were cultured in FreeStyle 293 Expression Medium (Gibco
177 12338018) supplemented with 1% penicillin–streptomycin (Gibco 15140-122). HEK293FT cells (Thermo
178 Fisher R70007) were cultured in Dulbecco's modified Eagle medium (DMEM, Gibco 31600-091)
179 supplemented with 10% fetal bovine serum (FBS) (Gibco 16140-071), 1% penicillin–streptomycin (Gibco
180 15140-122) and 4 mM additional L-glutamine (Gibco 25030-081). HEK293T Lenti-X cells (Takara 632180)
181 were cultured in HEK293FT media formulation supplemented with 1 mm sodium pyruvate from Gibco
182 (11360070). Jurkat T cells (ATCC TIB-152) were cultured in Roswell Park Memorial Institute medium (RPMI
183 1640, Gibco 31800-105) supplemented with 10% FBS, 1% penicillin–streptomycin, and 4 mM L-glutamine.
184 Sublines generated from these cell lines were cultured in the same way. Cells were subcultured at a 1:5 or
185 1:10 ratio every 2–3 days, using trypsin–EDTA (Gibco 25300-054) to remove adherent cells from the plate.
186 Freestyle 293-F cells were maintained at 37 °C with 8% CO_2 rotating at 135 rpm on a shaking platform
187 (Infors HT Multitron – I8000A) with orbital diameter 25 mm. HEK293FT, HEK293T Lenti-X, and Jurkat cells
188 were maintained at 37 °C with 5% CO_2. Freestyle 293F, HEK293FT, HEK293T Lenti-X and Jurkat cells
189 tested negative for mycoplasma with the MycoAlert Mycoplasma Detection Kit (Lonza LT07-318). HEK293T

190 Lenti-X and Jurkat cells tested negative for mycoplasma with the MycoAlert Mycoplasma Detection Kit
191 (Lonza LT07-318).
192
193 ***Cell line generation***
194 To generate lentivirus, HEK293T Lenti-X cells were plated in 10 cm dishes at a density of 5×10^6 cells per
195 dish (6.25×10^5 cells per ml). About 24 h later for Lenti-X, cells were transfected with 10 µg of lentiviral
196 transfer vector plasmid, 8 µg of psPAX2 second generation lentiviral packaging plasmid, and 3 µg pMD2.G
197 VSV-G-encoding plasmid via calcium phosphate transfection. Briefly, DNA was diluted with sterile H_2O and
198 added to $CaCl_2$ (2 M) to achieve a final concentration of 0.3 M $CaCl_2$. DNA-containing samples were then
199 added dropwise to an equal-volume of 2X HEPES-buffered saline (280 mM NaCl, 0.5 M HEPES, 1.5 mM
200 Na_2HPO_4) and pipetted four times to mix. After 3–4 min, the solution was vigorously pipetted eight times
201 and 2 mL of transfection reagent per 10 cm dish was added dropwise to cells. The plates were gently swirled
202 and incubated overnight at 37°C with 5% CO_2. The medium was replaced the morning after transfection
203 and cells were incubated for an additional 28–30 h. At 28 h post-medium change, lentivirus was collected
204 from the conditioned medium. The medium was centrifuged at 500 x *g* for 2 min to clear cells, and the
205 supernatant was filtered through a 0.45 µm PES pore filter (VWR). Lentivirus was concentrated from the
206 filtered supernatant by ultracentrifugation in Ultra Clear tubes (Beckman Coulter 344059) at 100,420 x *g* at
207 4 °C in a Beckman Coulter Optima L-80 XP ultracentrifuge using an SW41Ti rotor. The supernatant was
208 aspirated, leaving virus in ~100 µl final volume (~100X concentration), and concentrated lentivirus was left
209 on ice for at least 30 min before resuspension, then used to transduce $\sim 1 \times 10^5$ cells, plated either at the
210 time of transduction or on the day before. When appropriate, drug selection began 2 d post transduction,
211 using antibiotic concentrations of 1 µg ml^{-1} puromycin (Invitrogen ant-pr) on HEK293FT cells or 0.2 µg ml^{-1}
212 puromycin on Jurkat cells. Cells were kept in antibiotics for at least 2 weeks with subculturing every 1–2 d.
213
214 ***Transfection***
215 For transfection of Freestyle 293-F cells, a transfection protocol previously used to make AAV from
216 suspension HEK cells was utilized.[51] Briefly, 3 d before transfection cells were plated in fresh FreeStyle 293
217 Expression Medium at a concentration of 1×10^6 cells per mL. On the day of transfection, Freestyle 293-F

218 cells were spun at 150g x 5 min and resuspended in fresh FreeStyle 293 Expression Medium. The cells
219 were counted and plated at a density of 1×10^6 cells per mL. Cells were transfected with 1.5 µg of DNA per
220 million cells by PEI transfection. Plasmid DNA was added to a volume of room temperature (~20°C)
221 FreeStyle 293 Expression Medium, corresponding to 5% of the total volume in the flask to be transfected.
222 The tube was mixed to evenly distribute plasmid DNA. 3 µg of PEI (Polysciences, Inc – 24765) per million
223 cells was added to the tube and vortexed. The tube was then incubated for 10 min at room temperature to
224 allow for precomplex formation and then added directly to the flask.
225
226 ***EV-AAV production, isolation, and concentration***
227 Freestyle 293-F producer cell lines were transfected as described in Transfection. For EV-AAVs, the AAV
228 vector plasmid (transfer), packaging plasmid (rep/cap), and adenoviral helper plasmid (pHelper) were
229 transfected in equal DNA mass ratios up to the maximum DNA amount for the mixture. In transfections used
230 to make EV-AAV vectors including two types of EV surface protein, the mass ratio of transfected plasmids
231 was 1:1:1:1.59:1.41 for the AAV vector plasmid (transfer), packaging plasmid (rep/cap), adenoviral helper
232 plasmid (pHelper), pMD2.G VSV-G plasmid, and Ultra-HEK plasmid respectively. For control vectors in
233 which one such EV surface protein was omitted, pcDNA was included instead (at the equivalent DNA mass)
234 to ensure the same total mass of DNA was transfected into each flask. In experiments comparing various
235 single EV surface functionalizations, an equivalent mass of plasmid encoding each surface protein was
236 used, with the remaining mass made up by the AAV vector plasmid (transfer), packaging plasmid (rep/cap),
237 adenoviral helper plasmid (pHelper) at equivalent mass ratios. For exact DNA doses, see **Supplementary**
238 **Data 3**. 3 d after transfection, EV-AAVs were collected from the conditioned medium by differential
239 centrifugation. Briefly, conditioned medium was cleared of debris by centrifugation at 300 x g for 10 min to
240 remove cells followed by centrifugation at 2,000 x g for 20 min to remove dead cells and apoptotic bodies
241 in a Sorvall Legend X1R Centrifuge (ThermoFisher Scientific 75004261) with a TX-400 4 x 400 mL Swinging
242 Bucket Rotor. All centrifugation steps were performed at 4 °C. The supernatant underwent tangential flow
243 filtration using a KrossFlo KR2i TFF System with a MICROKROS 20CM 500KD filter (Repligen C02-S500-
244 05-S). Supernatant was flowed through the system at 24.99 mL/min at a constant transmembrane pressure
245 of 6.0 psi. The supernatant was concentrated to approximately 5 mL by TFF. In between samples, the TFF

246 was cleaned with at least 50 mL of 0.2 M NaOH that was sterile filtered by a 0.22 μm bottle top filter (Corning
247 431118). The system was then washed with at least 100 mL of PBS filtered by a 0.1 μm bottle top filter
248 (Corning 431475). The TFF system was kept in 0.05% sodium azide (EMD SX0299-1) in H_2O to prevent
249 contamination. After TFF, the EV-AAVs were further concentrated to approximately 0.5 mL (~800X
250 concentration) in Amicon Ultra-4 100K Centrifugal Filters (Millipore UFC810024) that were pre-washed with
251 0.1 μm bottle top filtered PBS. 0.5 mL of concentrated EV-AAVs were treated with Benzonase (25 U/mL,
252 EMD Millipore 70664) supplemented with $MgCl_2$ at a concentration of 2 mM for 1 h at 37 °C. Samples were
253 then purified to remove free AAV and other non-EV proteins using one of the methods below.
254
255 ***EV iodixanol purification***
256 Iodixanol gradient purification of EVs was modified from a previous report.[21] Briefly, 1x PBS-MK buffer was
257 prepared by dissolving 26.3 mg of MgCl2 and 14.91 mg of KCl in 100 mL of 1x PBS. The solution was
258 sterilized by passing it through a 0.22 μm filter (Corning 431118). 1 M NaCl/PBS-MK buffer was prepared
259 by dissolving 5.84 g of NaCl, 26.3 mg of MgCl2 and 14.91 mg of KCl in 1X PBS in a final volume of 100
260 mL. The solution was sterilized by passing it through a 0.22 μm filter (Corning 431118). Three iodixanol
261 (Sigma Alrich D1556) gradients were prepared from these solutions: 25% iodixanol (5 mL of 60% iodixanol,
262 7 mL of 1x PBS-MK buffer), 40% iodixanol (6.7 mL of 60% iodixanol and 3.3 mL of 1x PBS-MK buffer) and
263 60% iodixanol (10 mL of 60% iodixanol). These solutions were layered into UltraClear tubes (Beckman
264 Coulter 344059) in the following order: 1 mL 60% iodixanol, 3 mL 40% iodixanol, and 5 mL 25% iodixanol.
265 EVs were layered on top of the 25% iodixanol layer. The tubes were spun in a Beckman Coulter Optima L-
266 80 XP ultracentrifuge with an SW41 Ti rotor at 190,000 x g for 3 h at 18°C. After the spin, EVs were visible
267 as a white band in the 25% layer and were removed with a syringe with 18G needle. To remove the iodixanol
268 from the EVs, EVs were placed in a new UltraClear tube and diluted in PBS. The tubes were spun at
269 120,000 x g for 90 min at 4 °C to pellet the EVs. After the spin, the supernatant was aspirated, and EV
270 pellets were left in ~100–200 μl of PBS. EVs were incubated on ice for at least 30 min after supernatant
271 removal before resuspension in a total of 500 μL of PBS.
272
273 ***EV size exclusion chromatography purification***

274 Size exclusion chromatography was performed using qEVoriginal (35 nm) Gen2 columns (Izon ICO-35)
275 attached to an Automatic Fraction Collector V1 (Izon). We followed the manufacturer's instructions by
276 equilibrating the SEC column in PBS sterilized with 0.1 μM bottle top filters (Corning 431475). 0.5 mL of
277 EVs were placed on the column and EV fractions 1-4 were collected. Fractions 1-4 were combined and
278 concentrated to approximately 250 μL in Amicon Ultra-4 100K Centrifugal Filters (Millipore UFC810024)
279 that were pre-washed with 0.1 μm bottle top filtered PBS.
280
281 ***EV concentration determination by Nanoparticle Tracking Analysis (NTA)***
282 EV concentration was determined by NanoSight analysis. Samples were diluted in PBS sterilized with 0.1
283 μM bottle top filters (Corning 431475) to concentrations on the order of 10^8 particles per ml for analysis.
284 NanoSight analysis was performed on an NS300 (Malvern), software version 3.4. Three 30 s videos were
285 acquired per sample using a 642 nm laser on a camera level of 14, an infusion rate of 30 and a detection
286 threshold of 7. Default settings were used for the blur, minimum track length and minimum expected particle
287 size. EV concentrations were defined as the mean of the concentrations calculated from each video. Size
288 distributions were generated by the software.
289
290 ***AAV crude cell lysate production***
291 AAV was harvested from the Freestyle 293-F cell lysates of cells transfected to make non-targeted EV-
292 AAVs (no EV surface modifications). Briefly, 72 h post-transfection the EV-AAV containing supernatant was
293 removed and the cells were resuspended and washed with PBS sterilized with 0.1 μM bottle top filters
294 (Corning 431475). The cells were spun at 1000 x g for 7 min in a Sorvall Legend X1R Centrifuge
295 (ThermoFisher Scientific 75004261) with a TX-400 4 x 400 mL Swinging Bucket Rotor. The supernatant
296 was removed, and the cells were mixed with AAV lysis buffer corresponding to 2% of the initial culture
297 volume. AAV lysis buffer was made by combining 2 mL of 5 M NaCl, 0.158 g Tris-HCl and H_2O up to 100
298 mL. The solution was pH-adjusted to 8.5 and sterile filtered by a 0.22 μm bottle top filter (Corning 431118).
299 The cell pellet resuspended in AAV lysis buffer was then frozen in a bath of dry ice and ethanol, followed
300 by thawing in a 37°C bead bath. After each thawing the solution was vortexed vigorously for 30 s. The cell
301 pellet underwent three rounds of freeze/thaws. Benzonase (50 U/mL, EMD Millipore 70664) was added to

302 the mixture and incubated for 30 min at 37°C. The solution was transferred to 1.5 mL microcentrifuge tubes
303 and spun at 7000 rpm for 15 min in a microcentrifuge (Eppendorf Centrifuge 5424). The supernatant,
304 clarified AAV crude lysate, was transferred to a clean microcentrifuge tube and stored at 4°C until further
305 processing.
306
307 ***AAV purification by iodixanol gradient centrifugation***
308 1x PBS-MK buffer was prepared by dissolving 26.3 mg of MgCl2 and14.91 mg of KCl in 100 mL of 1x PBS.
309 The solution was sterilized by passing it through a 0.22 µm filter (Corning 431118). 1 M NaCl/PBS-MK buffer
310 was prepared by dissolving 5.84 g of NaCl, 26.3 mg of MgCl2 and 14.91 mg of KCl in 1X PBS in a final
311 volume of 100 mL. The solution was sterilized by passing it through a 0.22 µm filter (Corning 431118). Four
312 iodixanol (Sigma Alrich D1556) gradients were prepared from these solutions: 15% iodixanol (4.5 mL of
313 60% iodixanol and 13.5 mL of 1 M NaCl/PBS-MK buffer), 25% iodixanol (5 mL of 60% iodixanol, 7 mL of 1x
314 PBS-MK buffer and 30 µL of phenol red), 40% iodixanol (6.7 mL of 60% iodixanol and 3.3 mL of 1x PBS-
315 MK buffer) and 60% iodixanol (10 mL of 60% iodixanol and 45 µL of phenol red). These solutions were
316 layered into UltraClear ultracentrifuge tubes (Beckman Coulter 344059) in the following order: 1.35 mL 60%
317 iodixanol, 1.35 mL 40% iodixanol, 1.6 mL 25% iodixanol, 2.7 mL 15% iodixanol, and up to 4 mL of AAV
318 Crude Lysate. The tubes were spun in a Beckman Coulter Optima L-80 XP ultracentrifuge with an SW41 Ti
319 rotor at 190,000 x g for 3 h at 18°C. AAV was removed by inserting a syringe with 18G needle at the border
320 between the 60% and the 40% iodixanol fractions, with the needle facing upward to the lower portion of the
321 40% iodixanol fraction where the viral particles accumulate. The entire 40% iodixanol layer (transparent)
322 was removed without disturbing the layer of protein contaminants that accumulate at the interphase
323 between the 40% and 25% iodixanol layers. To remove the iodixanol this layer was mixed 1:1 by volume
324 with PBS and added to an Amicon Ultra-15 100K spin filter. The spin filter was spun at 3000 x g until the
325 volume remaining in the column was less than 1 mL. PBS was added to the column to the full volume and
326 spun at 3000 x g until 1 mL remained in the column. This was PBS washing was repeated 4 more times to
327 remove iodixanol and concentrate the AAV to its final volume.
328
329 ***AAV purification by magnetic beads***

330 Free AAV was purified using Dynabeads Capture Select AAVX Magnetic Beads (Thermofisher Scientific
331 2853522001) by the manufacturer's protocol. Briefly, 40 µL of bead slurry was added to a low protein binding
332 microcentrifuge tube with 460 µL of PBS. The tubes were placed on a magnetic stand and once the beads
333 were collected on the side of the tube the supernatant was removed. The beads were then mixed with 500
334 µL of PBS, the tubes were placed on a magnetic stand, and the supernatant was removed. 1 mL of AAV
335 crude lysate was added to the beads and the tubes were put on a rotating platform to continuously mix the
336 beads and lysate for 30 min. After 30 min the beads were collected with the magnetic stand and the
337 supernatant was removed. 500 µL of PBS was mixed with the beads, the beads were collected on the
338 magnetic stand, and the supernatant was removed. This PBS wash was repeated again. 20–50 µL of elution
339 buffer was added to the beads and mixed well. The elution buffer (50 mM citric acid, pH 2.5–3.0) and beads
340 were incubated at room temperature for 10 min with occasional pipetting. The beads were collected on the
341 magnetic stand and the supernatant containing purified AAV was collected. The eluted AAV mixture was
342 neutralized by adding 1 µL of Neutralization Buffer (1 M Tris-HCl, pH 8.7) for each 10 µL of eluate.
343
344 ***Physical titer determination by qPCR***
345 First, 5 µL of the EV-AAV, purified AAV, or clarified crude lysate samples were mixed with 37 µL nuclease-
346 free H_2O, 5 µL of 10x DNaseI buffer (ThermoFisher B43) and 1 µL of DNaseI (ThermoFisher EN0521) to
347 eliminate plasmid DNA, incubating at 37°C for 1 h followed by a 15 min inactivation step at 75°C. Samples
348 were placed on ice. Then, viral genomic DNA (vgDNA) was extracted using the High Pure Viral Nucleic Acid
349 Kit (Roche 11858874001), following manufacturer instructions. qPCR analysis was performed by amplifying
350 a sequence within the LumiScarlet reporter using primers CAGGGAGGTTTGACCAGTTT (forward), and
351 GGATATCGATCTTCAGCCCATT (reverse) or the mCherry reporter using the primers
352 AGGACGGCGAGTTCATCTA (forward), and CCCATGGTCTTCTTCTGCATTA (reverse). Primers were
353 designed using IDT's PrimerQuest Tool. A plasmid containing the LumiScarlet transgene (pJB035) or
354 mCherry transgene (pJB040) were used as a standard; serial dilutions were prepared using EASY dilution
355 (Takara Bio 9160), plating each dilution in duplicate. The vgDNA samples were diluted in nuclease free
356 H_2O, plating 4 serial dilutions per sample (in duplicate). For each qPCR reaction (each in a 96-well), 5 µL
357 of vgDNA sample were mixed with 10 µL Universal SYBR Master Mix 2x (ThermoFisher K0221), 0.15 µL

358 of 100 µM forward primer, 0.15 µL of 100 µM reverse primer, and 4.7 µL of nuclease free H_2O. qPCR plates
359 were sealed and spun at 500 x g for 2 min before placing in Bio-Rad C1000 Thermal Cycler with CFX96
360 Real-Time System. Samples run to detect LumiScarlet were heated to 98°C for 3 min, followed by 40 cycles
361 of: 98°C for 15 s, 62°C for 30 s. Then, a final step of 0.5°C increments every 5 s from 65°C to 95°C was
362 performed. Samples run to detect mCherry were heated to 98°C for 3 min, followed by 40 cycles of: 98°C
363 for 15 s, 55°C for 30 s. Then, a final step of 0.5°C increments every 5 s from 65°C to 95°C was performed.
364
365 ***Transduction assays***
366 For most experiments, EV-AAV or free AAV vectors were diluted in 0.1 µm bottle top filtered PBS so that
367 100 µL of the dilution contained 10^9 vector genomes. 100 µL of the diluted vector was added to each well
368 of a 24-well plate. Recipient cells were diluted to 10^4 cells per 900 µL of media and added to the wells with
369 vector, for a final dosage of 10^5 vector genomes per cell. Negative control wells received 100uL of 0.1 µm
370 bottle top filtered PBS. After the addition of all vectors and recipient cells, the plate was vigorously mixed
371 and placed in an incubator. 5 d post transduction, cells were harvested for flow cytometry using 0.05%
372 Trypsin-EDTA with phenol red for HEK293FT recipient cells for 5 min followed by quenching with medium.
373 The resulting cell solution was added to at least 2 volumes of FACS buffer (PBS pH 7.4, 2–5 mM EDTA,
374 0.1% BSA) supplemented with DAPI (to identify live cells) at a final concentration of 3 µM. Jurkat cells were
375 pipetted from the plate directly into FACS tubes containing FACS buffer supplemented with DAPI. A single
376 FACs tube of PBS treated cells was added to a tube containing FACS buffer without DAPI to identify live
377 cells (DAPI negative). Cells were centrifuged (150 × g for 5 min), supernatant was decanted, fresh FACS
378 buffer, with or without DAPI, was added, and cells were resuspended by briefly vortexing.
379
380 For experiments involving lentiviral transduction of HEK293T and HEK293FT by lentiviral vectors including
381 Ultra-HEK, similar methods were used. Cell lines were harvested, counted, and plated in 96-well, TC
382 treated, PBS-moated, flat-bottom plates at a density of 10^5 cells/mL in a volume of 100 µL per well (10^4
383 cells/well). Crude LV supernatant was diluted 5-fold seven times in complete DMEM to generate a seven-
384 point dilution curve starting from the first dilution. Cells were transduced by adding 100 µL/well of LV (each
385 dilution) and were incubated for 3 d at 37°C. Before analysis of transduction by flow cytometry, cells were

386 harvested by aspirating the media, trypsinizing cells for 5 min at room temperature, quenching with
387 complete DMEM, transferring lifted cells to a non-treated, round-bottom 96-well plate, spinning cells at 150
388 x g for 5 min, and resuspending in 30 µL of FACS buffer (PBS pH 7.4 with 0.05% BSA and 2 mM EDTA) +
389 DRAQ7 viability dye (Thermo Fisher D15106, diluted 1000x). DRAQ7 was used to identify live cells (DRAQ7
390 negative) for analysis.
391
392 ***Microscopy imaging***
393 Microscopy was conducted on a Keyence BZ-X800E fluorescence microscope and a Nikon CFI S Plan
394 Fluor ELWD 20XC objective (MRH08230). LumiScarlet fluorescence was imaged with a Keyence BZ-X
395 Filter TexasRed (Keyence, OP-87765). Images were taken using the Keyence BZ Series Viewer Software
396 (Version 01.03.00.01) in high resolution mode. Scale bars were added to images with the BZ-X800 Analyzer
397 Software (Version 1.1.2.4).
398
399 ***Lentiviral vector production for Ultra-HEK analysis***
400 Lentivirus (LV) samples were produced in adherent Lenti-X cells seeded at a density of 3.2 x 10^5 cells/mL
401 in a volume of 0.5 mL DMEM in 24-well TC-treated plates 24 h prior to transfection. Cells were transfected
402 with 0.4 µg total DNA comprising 50% transfer vector, 29% gag/pol, 16% rev, and 5% VSV-G for the VSV-
403 G only composition and 46% transfer vector, 29% gag/pol, 16% rev, 5% VSV-G, and 4% Ultra-HEK for the
404 VSV-G and Ultra-HEK composition. The transfer vector used encodes constitutive expression of
405 mNeonGreen. Plasmids used for lentivirus production are Syenex's commercial plasmids: SNX-mNG-TV3,
406 SNX-Gagpol, SNX-Rev, SNX-VSV-G, and Ultra-HEK. Ultra-HEK is a plasmid designed to increase lentiviral
407 transduction of HEK293-derived cells. Plasmids and PEI MAX transfection reagent (Polysciences 24765)
408 were diluted in Opti-MEM and mixed in equal volumes at a 4:1 mass ratio of PEI to DNA and complexed
409 for 24 min prior to transfection. Medium was changed 12–16 h later. At least 28 h post media change, LV
410 was harvested from the conditioned medium and centrifuged at 1000 x g for 10 min at 4°C, then aliquoted
411 and stored at -80°C until use.
412
413 ***Analytical flow cytometry and analysis***

414 Most flow cytometry was performed on a BD LSR Fortessa Special Order Research Product using the
415 552 nm laser for mCherry or LumiScarlet (610/20 filter) and the 488 nm laser for eGFP or mNeonGreen
416 (530/30 filter). At least 10,000 live cells were collected per sample for analysis. Data were analyzed using
417 FlowJo v10 (FlowJo, LLC). Briefly, cells were identified using a forward scatter area (FSC-A) versus side
418 scatter area (SSC-A) plot and gated for single cells using an FSC-A versus forward scatter height (FSC-H)
419 plot (**Supplementary Information (Figures S1,S2)**). Live single cells were identified using a DAPI-A versus
420 SSC-A plot. Gene delivery was determined by the percentage of live single cells that were brighter than
421 approximately the 0.1% of the brightest cells in the untransduced (PBS treated) cell samples (**Figure S1**).
422 Protein delivery was quantified by the mean of PE-Texas Red fluorescence of live single cells. This mean
423 fluorescence intensity was converted to MEPTRs by using UltraRainbow Calibration Particles (Spherotech).
424 Briefly, to determine the conversion from the arbitrary unit (au) of fluorescence recorded by the flow
425 cytometer to a standardized fluorescence unit (Molecules of Equivalent PE-TexasRed (MEPTR)),
426 UltraRainbow Calibration Particles were run as part of each flow cytometry experiment, except the AAV-
427 LumiScarlet experiment (**Figure 1**). This reagent contains nine subpopulations of beads, each of a specific
428 size and with a known intensity of various fluorophores, which are provided with calibration data for each
429 lot. The total bead population was identified by SSC-A vs. FSC-A gating, and subpopulations were identified
430 through two fluorescent channels (**Figure S3**). A calibration curve was generated for the experimentally
431 determined au vs. manufacturer supplied MEPTR, and a linear regression was performed with the
432 constraint that 0 au equals 0 MEPTR. The slope from the regression was used as the conversion factor.
433
434 For experiments involving lentiviral transduction of HEK293T and HEK293FT by Ultra-HEK, similar methods
435 were used. Flow cytometry was performed on a Novocyte Penteon using the 488 nm laser for mNeonGreen
436 (525/45 filter) and the 637 nm laser for DRAQ7 (725/40 filter). Approximately 3,000 live cells were collected
437 per sample for analysis. Data were analyzed using FlowJo v10 (FlowJo, LLC). Briefly, cells were identified
438 using an FSC-A vs SSC-A plot and gated for singlets using an FSC-A vs FSC-H plot. Live cells were
439 identified using a DRAQ7 negative gate drawn on a non-DRAQ7-stained sample, and transduced cells
440 were identified by drawing an mNeonGreen positive gate on a non-transduced sample.
441

442 ***Transmission Electron Microscopy (TEM)***

443 For transmission electron microscopy (TEM), samples were diluted in PBS sterilized with 0.1 µm bottle top
444 filters (Corning 431475) to concentrations on the order of 10^8 particles per µL as determined by Nanoparticle
445 Tracking Analysis. Grids were plasma treated, and 3 µL of diluted sample were placed on the carbon side
446 of the grid for 30 s. The grids were then briefly washed on 3 droplets of distilled water and placed on a
447 droplet of stain solution (2% ammonium molybdate) for a few seconds. The staining solution was blotted
448 off and the grid was placed on a second droplet of staining solution for 30 s. Finally, the excess staining
449 solution was removed, and the grid was air-dried. Samples were observed with a JEOL 3200FS TEM at an
450 acceleration voltage of 300 kV. A K2 camera was used for recording images.

451

452 ***Western blots***

453 For western blots comparing protein in cell lysates and protein in vesicles, a fixed number of vesicles and
454 a fixed mass of cell lysate were loaded into each well: 4.5×10^8 EVs/lane and 2 µg protein/lane,
455 respectively. An established western blot protocol[48] was followed with the following modifications. In most
456 cases, the following reducing Laemmli composition was used to boil samples (60 mM Tris-HCl pH 6.8, 10%
457 glycerol, 2% sodium dodecylsulphate, 100 mM dithiothreitol (DTT) and 0.01% bromophenol blue); in some
458 cases, a nonreducing Laemmli composition (without DTT) was used, as previously reported[52]. After transfer,
459 membranes were blocked whilst rocking for 1 h at room temperature in 5% milk in Tris-buffered saline with
460 Tween (TBST) (pH: 7.6, 50 mm Tris, 150 mm NaCl, HCl to pH 7.6, 0.1% Tween 20). Primary antibody was
461 added in 5% milk in TBST, rocking, for 1 h at room temperature and then washed three times with TBST
462 for 5 min each. Secondary antibody in 5% milk in TBST was added at room temperature for 1 h or overnight
463 at 4°C. Membranes were then washed three times with TBST for 5 min each. The membrane was incubated
464 with Clarity Western ECL substrate (Bio-Rad, #1705061) and imaged on an Azure c280 running Azure
465 cSeries Acquisition software v1.9.5.0606. Specific antibodies, antibody dilution, heating temperature,
466 heating time and Laemmli composition for each antibody was used as previously reported[52].

467

468 ***Statistical analysis***

469 Statistical tests employed are described in relevant figure legends. Unless otherwise stated, three
470 independent technical replicates were analyzed per condition, and the mean fluorescence intensity of at
471 least 10,000 live single cells were analyzed per sample. Each figure represents a single experiment that
472 was repeated (biological replicate) at least twice. Unless otherwise indicated, error bars represent the
473 standard error of the mean. GraphPad Prism 10 was used to analyze the data. Multicomparison statistical
474 analysis was performed using a one-way ANOVA test, followed by Tukey's multiple comparison (i.e.,
475 honestly significant difference, HSD) test to evaluate specific comparisons. Significance threshold:
476 $*p < 0.05$, $**p < 0.01$, $***p < 0.001$, $****p < 0.0001$.
477
478 **RESULTS**
479
480 **Distinguishing protein delivery from gene delivery by EV-AAV is challenging**
481 We first sought to quantify the magnitude and dynamics of pseudotransduction for EV-AAV delivery
482 to HEK293FTs. It is commonly expected that the fluorescence conferred to recipient cells by EV-mediated
483 delivery of producer cell-derived protein (i.e., pseudotransduction) will decrease over time due to protein
484 degradation and/or cell division, while fluorescence originating from true transduction (gene delivery and
485 resulting transgene expression in recipient cells) will persist and increase to steady state. However, the
486 dynamics of such contributions are poorly explored and are likely to be system specific. To characterize
487 these phenomena in our model system, we utilized an AAV vector that constitutively expresses a bright
488 fluorescent protein, LumiScarlet, and we generated both EV-AAV and free AAV preparations (**Figure S4**).
489 As a control for protein delivery, we included conditions lacking Rep and Cap genes ("No Rep/Cap"). We
490 also investigated several EV purification methods, reasoning that some fluorescent protein made by
491 producer cells may be excreted into the media along with free AAVs and EVs, and different EV purification
492 methods may remove these free proteins to different extents. Both purification methods yielded EVs with
493 expected protein markers (**Figures S5A,B**), appropriate size distributions (**Figure S5C**), and morphology
494 by TEM (**Figure S5D**). Purified vectors were dose-normalized (by genome count for EV-AAV and AAV with
495 No Rep/Cap EVs matched to EV-AAV by particle count) and delivered to HEK293FT cells (which actively
496 endocytose EVs). Fluorescence was monitored over 7 days by flow cytometry (**Figure 1**) and microscopy

497 (**Figure S6**). In general, fluorescence attributable to EV-AAV transduction was not readily distinguished
498 from fluorescence attributable to protein delivery (e.g., No Rep/Cap control). Free AAV2 conferred
499 distinguishable transgene expression, which was distinguished by quantifying the magnitude of
500 fluorescence per cell (**Figure 1A, right**). Representative histograms of LumiScarlet fluorescence from each
501 sample also demonstrate that fluorescence attributable to EV-AAV transduction was not readily
502 distinguished from fluorescence attributable to protein delivery (**Figure 1B**). This was visually confirmed by
503 microscopy (**Figure S6A-C**), in which free AAV2 conferred the expected whole cell fluorescence, while EV
504 conditions exhibit puncta that are readily apparent at 3 days post-treatment and remain detectable at 7
505 days post-treatment. Our analyses indicate that delivered protein is detectable in recipient cells for up to a
506 week, such that the time scale for delivered protein depletion and degradation is not readably separated
507 from the timescale of AAV episomal vector dilution (which may be particularly pronounced in these rapidly
508 dividing recipient cells). Overall, protein delivery by EV-AAVs may lead to significant pseudotransduction
509 and is challenging to distinguish from gene delivery regardless of EV purification method.
510

511 **A Cre recombinase-based dual reporter system enables discrimination between protein and gene**
512 **delivery**

513 To address the challenge of pseudotransduction, we developed a novel Cre recombinase (Cre)-
514 based system to enable quantitative and unambiguous evaluation of gene and protein delivery by EV-AAVs.
515 We utilized a Cre-responsive AAV genome encoding a constitutive mCherry fluorescent protein that, upon
516 recombination, is excised to instead drive expression of a green fluorescent protein.[47] This dual-
517 fluorescence system enables visualization of producer cell-derived protein delivery (mCherry) and gene
518 delivery (green) in Cre-expressing recipient cells (**Figure 2A**). Given a preceding Cre-responsive construct
519 developed for a distinct purpose[47], we generated several vectors to identify design choices that are useful
520 for this application (**Figure 2B**). We explored changing the gene delivery reporter from eGFP to
521 mNeonGreen, hypothesizing that a brighter fluorophore would help identify gene delivery. We also
522 hypothesized that removing the nuclear localization sequences (NLS) from the gene delivery reporter
523 protein may increase accumulation in the recipient cell, again facilitating detection. To evaluate these
524 designs, we made Cre-expressing recipient HEK293FT cells by lentiviral transduction.

525 Using this system, we evaluated protein and gene delivery by each reporter vector. Each variant
526 was packaged as either AAV2 crude lysate—which should include a mix of free AAV2 and cell-derived
527 fluorescent protein—or a no Rep/Cap control which should include only cell-derived fluorescent protein;
528 each was delivered to Cre-expressing recipient cells. Removal of the 3 x NLS generally increased mCherry
529 protein delivery, as expected, since the NLS sequesters some protein in the nucleus of the producer cells
530 (**Figure 2C**). Greater mCherry fluorescence was observed in Cre-negative than Cre-positive recipient cells,
531 suggesting that in the absence of Cre, more mCherry gene expression occurs in recipient cells. Most
532 importantly, green fluorescent protein was detected only with AAV2 preps (i.e., transduction-competent
533 vectors) and in Cre-expressing recipient cells (**Figure 2D**), validating this reporter system for
534 unambiguously indicating transduction and de novo transgene expression in recipient cells. Overall, the
535 mNeonGreen vectors conferred higher percentages of green positive live cells than did eGFP vectors, with
536 the mNeonGreen vector without an NLS performing the best. On balance, going forward we selected the
537 vector with mNeonGreen and the 3 x NLS, since it conferred more green-positivity in Cre-expressing
538 recipient cells compared to eGFP vectors (i.e., greater signal), and it conferred less mCherry fluorescence
539 compared to vectors without an NLS (i.e., lower background). We carried this validated reporter system
540 forward to probe EV-AAV bioengineering questions.
541
542 **EV-AAV2 surface functionalization substantially increases protein delivery but not gene delivery to**
543 **HEK293FTs**
544 We next investigated how EV functionalization strategies that have been reported to increase
545 delivery of lentiviruses or EVs impact protein and gene delivery by EV-AAV. VSV-G is often used in
546 pseudotyping lentiviruses[53,54] and EVs[55,56], and it increases the protein delivered by EVs.[56] VSV-G binds to
547 the LDL receptor (LDL-R) on the surface of recipient cells[31], increasing particle uptake as a result. Within
548 the low pH of the endosome, VSV-G undergoes conformational changes that enable it to promote fusion
549 between the viral (or EV) membrane and the endosomal membrane to release the vector's luminal contents
550 into the cytosol of the recipient cell.[57] Interestingly, a prior report indicated that pseudotyping EV-AAV2 with
551 VSV-G decreased the transduction of HEK293 cells compared to non-targeted EV-AAV2.[30] However, this
552 analysis employed a luminescence-based plate reader assay that may have been confounded by

553 pseudotransduction artifacts of protein delivery by the EV-AAVs. To separate the impacts of enhancing
554 uptake and mediating fusion, we also utilized Ultra-HEK, a commercial product (Syenex) that increases
555 lentiviral transduction of HEK293-based cells when combined with a fusogen such as VSV-G. Ultra-HEK is
556 described as interacting with proteins on the surface of recipient HEK293 cells to cause increased uptake
557 of the particle (but not fusion). In our hands, packing lentiviral vectors with Ultra-HEK led to increased gene
558 delivery (i.e., functional titer) for delivery to both HEK293T cells and HEK293FT cells (**Figure 3A–C**).
559 Using our reporter system and this menu of surface functionalization strategies (**Figure 3D**), we
560 revisited the question of how driving EV-AAV uptake (and/or fusion) impacts transduction efficiency. All
561 functionalization strategies increased protein delivery, likely due to increased particle uptake by recipient
562 cells (**Figure 3E**). Ultra-HEK combined with VSV-G functionalization increased protein delivery to the
563 greatest extent compared to non-targeted EV-AAV2. Since doses of EV-AAVs were normalized by genome
564 copy, it is possible that equivalent genome doses comprise distinct numbers of EVs. To exclude the
565 possibility that this could explain the protein delivery trend, we plotted protein delivery by EV dose (in particle
566 count), and we found that this does not well explain our observations (**Figure S7**). Thus, differences in
567 protein delivery are best explained by the biological effects of our functionalization strategies. Interestingly,
568 surface functionalization did not increase gene delivery to the same degree as it did protein delivery (**Figure**
569 **3F**). Only the dual functionalization strategy modestly increased the amount of gene delivery to HEKs over
570 non-targeted vectors, and there was no evidence that fusion mediated by VSV-G enhanced or blocked EV-
571 AAV gene delivery. This led us to investigate whether these trends extend to other serotypes and recipient
572 cells.
573
574 **EV-AAV6 surface functionalization increases protein and gene delivery to Jurkat T cells**
575 We next explored EV-AAV delivery to a cell type with low spontaneous EV uptake. We chose to
576 use human Jurkat T cells, which are somewhat recalcitrant to EV-based delivery due (at least in part) to
577 low endocytosis.[28] We transduced Jurkats with the Cre recombinase gene to make a recipient line
578 compatible with our dual reporter system. We used AAV6 as it infects both primary T cells[59] and Jurkats[60].
579 We focused on VSV-G functionalization which mediates lentiviral transduction via LDL-R binding and
580 uptake (**Figure 4A**).[61] Similar to HEK293FT delivery (**Figure 3**), VSV-G functionalization increased protein

581 delivery to Jurkats compared to non-targeted EV-AAV6 (**Figure 4B**). Surprisingly, and unlike in HEK293FT
582 recipient cells, VSV-G functionalization also increased gene delivery to Jurkats (**Figure 4C**). This led us to
583 investigate what mechanism conferred by VSV-G (uptake vs. fusion) contributed to increased gene delivery.
584 We employed two VSV-G mutants to dissect these mechanisms (**Figure 4D**). P127D retains the ability to
585 bind to LDL-R but is deficient in membrane fusion.[49,62,63] Conversely, mutations K47Q-R354A block LDL-R
586 binding but still enable VSV-G to confer membrane fusion.[64-66] Wild-type (WT) and P127D VSV-G vectors
587 delivered more protein than did K47Q-R354A or non-targeted vectors (**Figure 4E**). Interestingly, the K47Q-
588 R354A VSV-G conferred less gene delivery than did the WT or P127D VSV-G vectors, indicating that
589 binding to LDL-R on recipient cells is the dominant mechanism by which VSV-G increases gene delivery to
590 Jurkat T cells (**Figure 4F**). Notably, P127D VSV-G, which is fusion incompetent, conferred more gene
591 delivery than did VSV-G WT vectors. Altogether, these results may indicate that for EV-AAV6 delivery to
592 Jurkats, increased LDL-R binding increases particle uptake and transduction, while membrane fusion limits
593 transduction.
594
595 **Recipient cell type but not capsid serotype drives the impact of functionalization on EV-AAV delivery**
596 To reconcile the distinct patterns observed in our HEK293FT and Jurkat delivery experiments, we
597 investigated whether differences are driven primarily by recipient cell type or AAV serotype. We chose to
598 investigate transducing HEK293FT cells with AAV6 since AAV6 is much less efficient at infecting
599 HEK293FTs compared to AAV2.[60] This difference may be due to differences in receptor density on the
600 surface of HEKs. AAV2 primarily uses heparan sulfate proteoglycan to mediate binding and uptake by
601 recipient cells.[67] In contrast, AAV6 primarily uses sialic acid as its receptor[67], which may be less abundant
602 or accessible on HEK293 cells compared to heparan sulfate proteoglycan. Therefore, we hypothesized that
603 increasing uptake of EV-AAV6 (e.g., via VSV-G functionalization) would increase transduction compared to
604 both non-targeted EV-AAV6 or free AAV6 (**Figure 5A**). VSV-G functionalization increased protein delivery
605 compared to non-targeted EV-AAV6, as expected (**Figure 5B**). However, VSV-G mediated uptake (and
606 fusion) did not increase gene delivery by EV-AAV6 (**Figure 5C**), as was seen for EV-AAV2 (**Figure 3F**).
607 Thus, increasing uptake and membrane fusion in a cell type that is permissible to EV delivery, such as
608 HEK293FTs, did not increase gene delivery regardless of AAV capsid choice. With the set of conditions

evaluated, EV surface functionalization strategies conferred cell type-dependent but not capsid-dependent effects on EV-AAV gene delivery.

DISCUSSION

Engineered EVs are promising delivery vehicles for AAV vectors, enabling tissue-specific targeting and neutralizing antibody evasion. However, analyzing and bioengineering such vectors is made challenging by the difficulty associated with distinguishing protein delivery (pseudotransduction) from gene delivery. To address this need, in this study we developed and validated a new assay that unambiguously distinguishes gene delivery from protein delivery, while enabling quantification of both phenomena. This assay helped to generate new insights that inform both interpretation of past studies and identify opportunities for future investigation.

Our observations provide new insights that help to interpret apparent contradictions in the EV-AAV literature. Some previous studies report that EV-AAVs are more potent than AAV vectors for *in vivo* delivery (on a per genome basis)[14-16,22], but other work focused on delivery to neuronal and primary astrocyte cell cultures seemingly contradicts this finding[68]. It is possible that improved *in vivo* efficacy of EV-AAV particles is primarily attributable not to the enhanced interaction between the AAV and the target cells, but rather to shielding of AAVs from neutralizing antibodies and/or biodistribution effects such as increased circulation time or improved delivery through tissue barriers. Our observations add another layer of possible explanation, given our finding that target cell type and capsid choice may impact the efficacy of EV-AAV compared to free AAV. Free AAV2 was significantly more potent for gene delivery to HEK293FTs compared to non-targeted EV-AAV2 (**Figure 3**). However, non-targeted EV-AAV6 outperformed free AAV6 in gene delivery to HEK293FTs (**Figure 5**). This suggests that capsid choice may impact the relative gene delivery efficacy of EV-AAV and free AAV. In contrast, EV-AAV6 outperformed free AAV6 in transduction of Jurkat T cells (**Figure 4**), suggesting that the target cell may also impact efficacy comparisons between EV-AAV and free AAV. Overall, our findings indicate that the impact of EV-encapsulation of AAV confers case-specific effects that should be evaluated for each application, and which may drive application-specific bioengineering.

636 This study focused on identifying high level determinants of functional delivery, yet it also identified
637 opportunities for further subsequent mechanistic investigations. Increasing the uptake of EV-AAV to
638 HEK293FT recipient cells, both with or without promoting membrane fusion, increased protein delivery, but
639 this did not substantially increase gene delivery for either AAV2 or AAV6. However, VSV-G functionalization
640 of EV-AAV6 increased both protein and gene delivery to Jurkat T cells, and this effect was driven primarily
641 by increased uptake rather than fusion; indeed, blocking VSV-G-mediated fusion enhanced gene delivery.
642 The basis for these differences is not known. A possible explanation is that AAV requires processing in the
643 endosome—including capsid cleavage by endosomal cathepsins[32] and acidification-mediated
644 autoproteolytic processing[33] to expose a phospholipase domain promoting virion escape and gene
645 delivery[34,35]. This requirement is well-characterized for free AAV2 and may extend to other serotypes. It
646 would be informative to probe how each step in capsid processing is impacted by encapsulation in EVs. In
647 addition, directly tracking internalization of both receptors and particles could help to test the mechanisms
648 offered as speculative explanations here. It will be interesting to extend these studies to the many AAV
649 capsid variants that exist, including natural serotypes as well as novel forms developed through directed
650 evolution and protein engineering[69], and to a variety of recipient cell types including those which endocytose
651 EVs more readily than do HEK293FTs[58]. This work could also enable new AAV bioengineering campaigns
652 specific to enhancing EV-AAV delivery, such as exploring mutations that destabilize the capsid structure to
653 enhance transduction after EV fusion and delivery of the AAV core to the cytosol, bypassing endosomal
654 processing.
655 An exciting prospect is extending this assay for *in vivo* EV-AAV delivery analyses. The stoplight vector
656 inspiring our approach was originally employed to detect Cre expression *in vivo*[47]. Given that transgenic
657 animals can be engineered to express Cre in a tissue-restricted or general fashion[70], our assay could be
658 employed to unambiguously identify EV-AAV gene delivery in vivo. Such a capability could be particularly
659 useful for directly comparing AAV and EV-AAV-mediated delivery, and for enabling comparative evaluation
660 of bioengineering approaches, *in vivo* multiplexed screening, and other efforts for which pseudotransduction
661 is misleading or reduces signal-to-noise to preclude feasibility. We expect that such work can help advance
662 the understanding and use of EV-AAV vectors for diverse gene delivery applications.
663

AUTHOR CONTRIBUTIONS

J.D.B., D.M.S., N.P.K., D.T.E., and J.N.L. conceived the initial project. J.D.B. performed the experiments. D.M.S. and H.I.E. performed the Ultra-HEK lentiviral vector experiment. J.D.B. and J.N.L. planned and analyzed experiments. J.D.B and J.N.L. wrote the manuscript. J.N.L. supervised the work.

ACKNOWLEDGEMENTS

J.D.B. was supported by the National Institutes of Health Training Grant (T32GM008449) through Northwestern University's Biotechnology Training Program. J.D.B was supported by the National Science Foundation Graduate Research Fellowship under grant number (DGE-1842165). This project was partially supported by an award from the McCormick Catalyst Fund (J.N.L.) and by a Cornew Innovation Award from the Chemistry of Life Processes Institute at Northwestern University (J.N.L.). Flow Cytometry was performed in the Northwestern University Flow Cytometry Core Facility supported by Cancer Center Support Grant (NCI CA060553) and in the Single Cell Genomics Facility at Northwestern University (RRID:SCR_026652), graciously supported by the Department of Neurobiology, the Department of Molecular Biosciences, and the NU Office for Research. This work made use of the BioCryo Core (RRID:SCR_021288) of Northwestern University’s NUANCE Center, which has received support from the SHyNE Resource (NSF ECCS-2025633), the IIN, and Northwestern's MRSEC program (NSF DMR-2308691). Biological analysis] was performed in the Analytical bioNanoTechnology Equipment Core Facility of the Center for Regenerative Nanomedicine at Northwestern University. ANTEC receives partial support from the Soft and Hybrid Nanotechnology Experimental (SHyNE) Resource (NSF ECCS-2025633) and Feinberg School of Medicine, Northwestern University. This work was supported by the Northwestern University Sanger Sequencing Facility. Any opinion, findings and conclusions or recommendations expressed in this material are those of the authors and do not necessarily reflect the views of the National Science Foundation. The authors kindly thank the Leonard lab members for useful discussions throughout the planning, experimental, analysis and writing phases of this project. The authors would like to thank Dmitriy Bobrovnikov and Roxi Mitrut for discussions of Cre-responsive AAV vectors.

DECLARATION OF INTERESTS STATEMENT

692 J.N.L., D.M.S. and H.I.E. have financial interests in Syenex Inc., which could potentially benefit from the
693 outcomes of this research.
694

695 **REFERENCES**

696 1 Wang, J.-H., Gessler, D. J., Zhan, W., Gallagher, T. L. & Gao, G. Adeno-associated virus as a
697 delivery vector for gene therapy of human diseases. *Signal Transduction and Targeted Therapy* **9**,
698 78 (2024). https://doi.org:10.1038/s41392-024-01780-w

699 2 Earley, J., Piletska, E., Ronzitti, G. & Piletsky, S. Evading and overcoming AAV neutralization in
700 gene therapy. *Trends in Biotechnology* **41**, 836-845 (2023).
701 https://doi.org:https://doi.org/10.1016/j.tibtech.2022.11.006

702 3 Srivastava, A. In vivo tissue-tropism of adeno-associated viral vectors. *Current Opinion in Virology*
703 **21**, 75-80 (2016). https://doi.org:https://doi.org/10.1016/j.coviro.2016.08.003

704 4 Duan, D. Lethal immunotoxicity in high-dose systemic AAV therapy. *Molecular Therapy* **31**, 3123-
705 3126 (2023). https://doi.org:https://doi.org/10.1016/j.ymthe.2023.10.015

706 5 Hordeaux, J. *et al.* High-dose systemic adeno-associated virus vector administration causes liver
707 and sinusoidal endothelial cell injury. *Molecular Therapy* **32**, 952-968 (2024).
708 https://doi.org:https://doi.org/10.1016/j.ymthe.2024.02.002

709 6 Raposo, G. & Stoorvogel, W. Extracellular vesicles: exosomes, microvesicles, and friends. *J Cell*
710 *Biol* **200**, 373-383 (2013). https://doi.org:10.1083/jcb.201211138

711 7 Cocucci, E., Racchetti, G. & Meldolesi, J. Shedding microvesicles: artefacts no more. *Trends Cell*
712 *Biol* **19**, 43-51 (2009). https://doi.org:10.1016/j.tcb.2008.11.003

713 8 Valadi, H. *et al.* Exosome-mediated transfer of mRNAs and microRNAs is a novel mechanism of
714 genetic exchange between cells. *Nat Cell Biol* **9**, 654-659 (2007). https://doi.org:10.1038/ncb1596

715 9 Mizrak, A. *et al.* Genetically engineered microvesicles carrying suicide mRNA/protein inhibit
716 schwannoma tumor growth. *Mol Ther* **21**, 101-108 (2013). https://doi.org:10.1038/mt.2012.161

717 10 Andaloussi, E. L., Mager, I., Breakefield, X. O. & Wood, M. J. Extracellular vesicles: biology and
718 emerging therapeutic opportunities. *Nature reviews. Drug discovery* **12**, 347-357 (2013).
719 https://doi.org:10.1038/nrd3978

720 11 Gyorgy, B., Hung, M. E., Breakefield, X. O. & Leonard, J. N. Therapeutic applications of
721 extracellular vesicles: clinical promise and open questions. *Annual review of pharmacology and*
722 *toxicology* **55**, 439-464 (2015). https://doi.org:10.1146/annurev-pharmtox-010814-124630

723 12 Marcus, M. E. & Leonard, J. N. FedExosomes: Engineering Therapeutic Biological Nanoparticles
724 that Truly Deliver. *Pharmaceuticals-Base* **6**, 659-680 (2013). https://doi.org:10.3390/ph6050659
725 13 Maguire, C. A. *et al.* Microvesicle-associated AAV vector as a novel gene delivery system. *Mol Ther*
726 **20**, 960-971 (2012). https://doi.org:10.1038/mt.2011.303
727 14 Hudry, E. *et al.* Exosome-associated AAV vector as a robust and convenient neuroscience tool.
728 *Gene Therapy* **23**, 380-392 (2016). https://doi.org:10.1038/gt.2016.11
729 15 György, B. *et al.* Rescue of Hearing by Gene Delivery to Inner-Ear Hair Cells Using Exosome-
730 Associated AAV. *Molecular Therapy* **25**, 379-391 (2017).
731 https://doi.org:https://doi.org/10.1016/j.ymthe.2016.12.010
732 16 Wassmer, S. J., Carvalho, L. S., György, B., Vandenberghe, L. H. & Maguire, C. A. Exosome-
733 associated AAV2 vector mediates robust gene delivery into the murine retina upon intravitreal
734 injection. *Scientific Reports* **7**, 45329 (2017). https://doi.org:10.1038/srep45329
735 17 Meliani, A. *et al.* Enhanced liver gene transfer and evasion of preexisting humoral immunity with
736 exosome-enveloped AAV vectors. *Blood Advances* **1**, 2019-2031 (2017).
737 https://doi.org:10.1182/bloodadvances.2017010181
738 18 Breuer, C. B. *et al.* In vivo engineering of lymphocytes after systemic exosome-associated AAV
739 delivery. *Scientific Reports* **10**, 4544 (2020). https://doi.org:10.1038/s41598-020-61518-w
740 19 Liu, B. *et al.* AAV-Containing Exosomes as a Novel Vector for Improved Gene Delivery to Lung
741 Cancer Cells. *Frontiers in Cell and Developmental Biology* **Volume 9 - 2021** (2021).
742 https://doi.org:10.3389/fcell.2021.707607
743 20 Kwak, G. *et al.* Extracellular vesicles enhance pulmonary transduction of stably associated adeno-
744 associated virus following intratracheal administration. *Journal of Extracellular Vesicles* **12**, 12324
745 (2023). https://doi.org:https://doi.org/10.1002/jev2.12324
746 21 Li, X. *et al.* Extracellular Vesicle–Encapsulated Adeno-Associated Viruses for Therapeutic Gene
747 Delivery to the Heart. *Circulation* **148**, 405-425 (2023).
748 https://doi.org:10.1161/CIRCULATIONAHA.122.063759

749 22 György, B., Fitzpatrick, Z., Crommentuijn, M. H. W., Mu, D. & Maguire, C. A. Naturally enveloped
750 AAV vectors for shielding neutralizing antibodies and robust gene delivery in vivo. *Biomaterials* **35**,
751 7598-7609 (2014). https://doi.org:https://doi.org/10.1016/j.biomaterials.2014.05.032
752 23 Cheng, M. *et al.* Neutralizing Antibody Evasion and Transduction with Purified Extracellular Vesicle-
753 Enveloped Adeno-Associated Virus Vectors. *Human Gene Therapy* **32**, 1457-1470 (2021).
754 https://doi.org:10.1089/hum.2021.122
755 24 Cheng, M. *et al.* Probing aspects of extracellular vesicle associated AAV allows increased vector
756 yield and insight into its transduction and immune-evasive properties. *Mol Ther Methods Clin Dev*
757 **33**, 101407 (2025). https://doi.org:10.1016/j.omtm.2025.101407
758 25 Espinoza, P. *et al.* Metabolic engineering improves transduction efficiency and downstream vector
759 isolation by altering the lipid composition of extracellular vesicle-enclosed AAV. *Metabolic*
760 *Engineering* **88**, 40-49 (2025). https://doi.org:https://doi.org/10.1016/j.ymben.2024.12.003
761 26 Alvarez-Erviti, L. *et al.* Delivery of siRNA to the mouse brain by systemic injection of targeted
762 exosomes. *Nat Biotechnol* **29**, 341-345 (2011). https://doi.org:10.1038/nbt.1807
763 27 Murphy, D. E. *et al.* Extracellular vesicle-based therapeutics: natural versus engineered targeting
764 and trafficking. *Experimental & molecular medicine* **51**, 1-12 (2019).
765 28 Stranford, D. M. *et al.* Genetically encoding multiple functionalities into extracellular vesicles for the
766 targeted delivery of biologics to T cells. *Nature Biomedical Engineering* **8**, 397-414 (2024).
767 https://doi.org:10.1038/s41551-023-01142-x
768 29 Wiklander, O. P. B. *et al.* Antibody-displaying extracellular vesicles for targeted cancer therapy.
769 *Nature Biomedical Engineering* **8**, 1453-1468 (2024). https://doi.org:10.1038/s41551-024-01214-6
770 30 Maguire, C. A. *et al.* Microvesicle-associated AAV Vector as a Novel Gene Delivery System.
771 *Molecular Therapy* **20**, 960-971 (2012). https://doi.org:https://doi.org/10.1038/mt.2011.303
772 31 Finkelshtein, D., Werman, A., Novick, D., Barak, S. & Rubinstein, M. LDL receptor and its family
773 members serve as the cellular receptors for vesicular stomatitis virus. *Proceedings of the National*
774 *Academy of Sciences* **110**, 7306-7311 (2013). https://doi.org:doi:10.1073/pnas.1214441110
775 32 Akache, B. *et al.* A two-hybrid screen identifies cathepsins B and L as uncoating factors for adeno-
776 associated virus 2 and 8. *Mol Ther* **15**, 330-339 (2007). https://doi.org:10.1038/sj.mt.6300053

33 Salganik, M. *et al.* Evidence for pH-dependent protease activity in the adeno-associated virus capsid. *J Virol* **86**, 11877-11885 (2012). https://doi.org:10.1128/jvi.01717-12

34 Girod, A. *et al.* The VP1 capsid protein of adeno-associated virus type 2 is carrying a phospholipase A2 domain required for virus infectivity. *J Gen Virol* **83**, 973-978 (2002). https://doi.org:10.1099/0022-1317-83-5-973

35 Stahnke, S. *et al.* Intrinsic phospholipase A2 activity of adeno-associated virus is involved in endosomal escape of incoming particles. *Virology* **409**, 77-83 (2011). https://doi.org:10.1016/j.virol.2010.09.025

36 Guo, Y. *et al.* Early events in rabies virus infection-Attachment, entry, and intracellular trafficking. *Virus Res* **263**, 217-225 (2019). https://doi.org:10.1016/j.virusres.2019.02.006

37 Gaudin, Y. Rabies Virus-Induced Membrane Fusion Pathway. *Journal of Cell Biology* **150**, 601-612 (2000). https://doi.org:10.1083/jcb.150.3.601

38 Albertini, A. A., Baquero, E., Ferlin, A. & Gaudin, Y. Molecular and cellular aspects of rhabdovirus entry. *Viruses* **4**, 117-139 (2012). https://doi.org:10.3390/v4010117

39 Haas, D. L., Case, S. S., Crooks, G. M. & Kohn, D. B. Critical Factors Influencing Stable Transduction of Human CD34+ Cells with HIV-1-Derived Lentiviral Vectors. *Molecular Therapy* **2**, 71-80 (2000). https://doi.org:https://doi.org/10.1006/mthe.2000.0094

40 Galla, M., Will, E., Kraunus, J., Chen, L. & Baum, C. Retroviral Pseudotransduction for Targeted Cell Manipulation. *Molecular Cell* **16**, 309-315 (2004). https://doi.org:https://doi.org/10.1016/j.molcel.2004.09.023

41 Nash, K. L. & Lever, A. M. L. Green fluorescent protein: green cells do not always indicate gene expression. *Gene Therapy* **11**, 882-883 (2004). https://doi.org:10.1038/sj.gt.3302246

42 Geering, B., Schmidt-Mende, J., Federzoni, E., Stoeckle, C. & Simon, H.-U. Protein overexpression following lentiviral infection of primary mature neutrophils is due to pseudotransduction. *Journal of Immunological Methods* **373**, 209-218 (2011). https://doi.org:https://doi.org/10.1016/j.jim.2011.08.024

803 43 Kim, J. T. *et al.* Dendritic cell–targeted lentiviral vector immunization uses pseudotransduction and
804 DNA-mediated STING and cGAS activation. *Science Immunology* **2**, eaal1329 (2017).
805 https://doi.org:doi:10.1126/sciimmunol.aal1329
806 44 Hung, M. E. & Leonard, J. N. A platform for actively loading cargo RNA to elucidate limiting steps
807 in EV-mediated delivery. *J Extracell Vesicles* **5**, 31027 (2016). https://doi.org:10.3402/jev.v5.31027
808 45 Somiya, M. & Kuroda, S. i. Verification of extracellular vesicle-mediated functional mRNA delivery
809 via RNA editing. *bioRxiv*, 2022.2001.2025.477620 (2022).
810 https://doi.org:10.1101/2022.01.25.477620
811 46 Yeh, H. W. *et al.* ATP-Independent Bioluminescent Reporter Variants To Improve in Vivo Imaging.
812 *ACS Chem Biol* **14**, 959-965 (2019). https://doi.org:10.1021/acschembio.9b00150
813 47 Bäck, S. *et al.* Neuron-Specific Genome Modification in the Adult Rat Brain Using CRISPR-Cas9
814 Transgenic Rats. *Neuron* **102**, 105-119.e108 (2019).
815 https://doi.org:https://doi.org/10.1016/j.neuron.2019.01.035
816 48 Donahue, P. S. *et al.* The COMET toolkit for composing customizable genetic programs in
817 mammalian cells. *Nature Communications* **11**, 779 (2020). https://doi.org:10.1038/s41467-019-
818 14147-5
819 49 Votteler, J. *et al.* Designed proteins induce the formation of nanocage-containing extracellular
820 vesicles. *Nature* **540**, 292-295 (2016). https://doi.org:10.1038/nature20607
821 50 Sauer, B. & Henderson, N. Targeted insertion of exogenous DNA into the eukaryotic genome by
822 the Cre recombinase. *New Biol* **2**, 441-449 (1990).
823 51 Blessing, D., Déglon, N. & Schneider, B. L. in *Recombinant Protein Expression in Mammalian Cells:*
824 *Methods and Protocols* (ed David L. Hacker) 259-274 (Springer New York, 2018).
825 52 Gunnels, T. F., Stranford, D. M., Mitrut, R. E., Kamat, N. P. & Leonard, J. N. Elucidating Design
826 Principles for Engineering Cell-Derived Vesicles to Inhibit SARS-CoV-2 Infection. *Small* **18**,
827 2200125 (2022). https://doi.org:https://doi.org/10.1002/smll.202200125
828 53 Gutierrez-Guerrero, A., Cosset, F.-L. & Verhoeyen, E. Lentiviral Vector Pseudotypes: Precious
829 Tools to Improve Gene Modification of Hematopoietic Cells for Research and Gene Therapy.
830 *Viruses* **12**, 1016 (2020).

831 54 Dautzenberg, I. J. C., Rabelink, M. J. W. E. & Hoeben, R. C. The stability of envelope-pseudotyped
832 lentiviral vectors. *Gene Therapy* **28**, 89-104 (2021). https://doi.org:10.1038/s41434-020-00193-y
833 55 Ma, D. *et al.* Engineered extracellular vesicles enable high-efficient delivery of intracellular
834 therapeutic proteins. *Protein & Cell* **15**, 724-743 (2024). https://doi.org:10.1093/procel/pwae015
835 56 Meyer, C. *et al.* Pseudotyping exosomes for enhanced protein delivery in mammalian cells. *Int J*
836 *Nanomedicine* **12**, 3153-3170 (2017). https://doi.org:10.2147/ijn.S133430
837 57 Kim, I. S. *et al.* Mechanism of membrane fusion induced by vesicular stomatitis virus G protein.
838 *Proceedings of the National Academy of Sciences* **114**, E28-E36 (2017).
839 https://doi.org:doi:10.1073/pnas.1618883114
840 58 Stranford, D. M., Hung, M. E., Gargus, E. S., Shah, R. N. & Leonard, J. N. A Systematic Evaluation
841 of Factors Affecting Extracellular Vesicle Uptake by Breast Cancer Cells. *Tissue Eng Part A* **23**,
842 1274-1282 (2017). https://doi.org:10.1089/ten.TEA.2017.0158
843 59 Wang, J. *et al.* Highly efficient homology-driven genome editing in human T cells by combining zinc-
844 finger nuclease mRNA and AAV6 donor delivery. *Nucleic Acids Research* **44**, e30-e30 (2015).
845 https://doi.org:10.1093/nar/gkv1121
846 60 Ellis, B. L. *et al.* A survey of ex vivo/in vitro transduction efficiency of mammalian primary cells and
847 cell lines with Nine natural adeno-associated virus (AAV1-9) and one engineered adeno-associated
848 virus serotype. *Virology Journal* **10**, 74 (2013). https://doi.org:10.1186/1743-422X-10-74
849 61 Gutierrez-Guerrero, A., Cosset, F. L. & Verhoeyen, E. Lentiviral Vector Pseudotypes: Precious Tools
850 to Improve Gene Modification of Hematopoietic Cells for Research and Gene Therapy. *Viruses* **12**
851 (2020). https://doi.org:10.3390/v12091016
852 62 Fredericksen, B. L. & Whitt, M. A. Vesicular stomatitis virus glycoprotein mutations that affect
853 membrane fusion activity and abolish virus infectivity. *Journal of Virology* **69**, 1435-1443 (1995).
854 https://doi.org:10.1128/jvi.69.3.1435-1443.1995
855 63 Liang, X. *et al.* Engineering of extracellular vesicles for efficient intracellular delivery of multimodal
856 therapeutics including genome editors. *Nature Communications* **16**, 4028 (2025).
857 https://doi.org:10.1038/s41467-025-59377-y

858 64 Nikolic, J. *et al.* Structural basis for the recognition of LDL-receptor family members by VSV
859 glycoprotein. *Nature Communications* **9**, 1029 (2018). https://doi.org:10.1038/s41467-018-03432-
860 4
861 65 Dobson, C. S. *et al.* Antigen identification and high-throughput interaction mapping by
862 reprogramming viral entry. *Nature Methods* **19**, 449-460 (2022). https://doi.org:10.1038/s41592-
863 022-01436-z
864 66 Gao, Y. & Bergman, I. Vesicular Stomatitis Virus (VSV) G Glycoprotein Can Be Modified to Create
865 a Her2/Neu-Targeted VSV That Eliminates Large Implanted Mammary Tumors. *Journal of Virology*
866 **97**, e00372-00323 (2023). https://doi.org:10.1128/jvi.00372-23
867 67 Issa, S. S., Shaimardanova, A. A., Solovyeva, V. V. & Rizvanov, A. A. Various AAV Serotypes and
868 Their Applications in Gene Therapy: An Overview. *Cells* **12** (2023).
869 https://doi.org:10.3390/cells12050785
870 68 Kovács, O. T. *et al.* Impact of Medium-Sized Extracellular Vesicles on the Transduction Efficiency
871 of Adeno-Associated Viruses in Neuronal and Primary Astrocyte Cell Cultures. *Int J Mol Sci* **22**
872 (2021). https://doi.org:10.3390/ijms22084221
873 69 Nisanov, A. M., de Jesús, J. A. R. & Schaffer, D. V. Advances in AAV capsid engineering: Integrating
874 rational design, directed evolution and machine learning. *Molecular Therapy* **33**, 1937-1945 (2025).
875 70 Kim, H., Kim, M., Im, S. K. & Fang, S. Mouse Cre-LoxP system: general principles to determine
876 tissue-specific roles of target genes. *Lab Anim Res* **34**, 147-159 (2018).
877 https://doi.org:10.5625/lar.2018.34.4.147

878

879

880 **FIGURES**

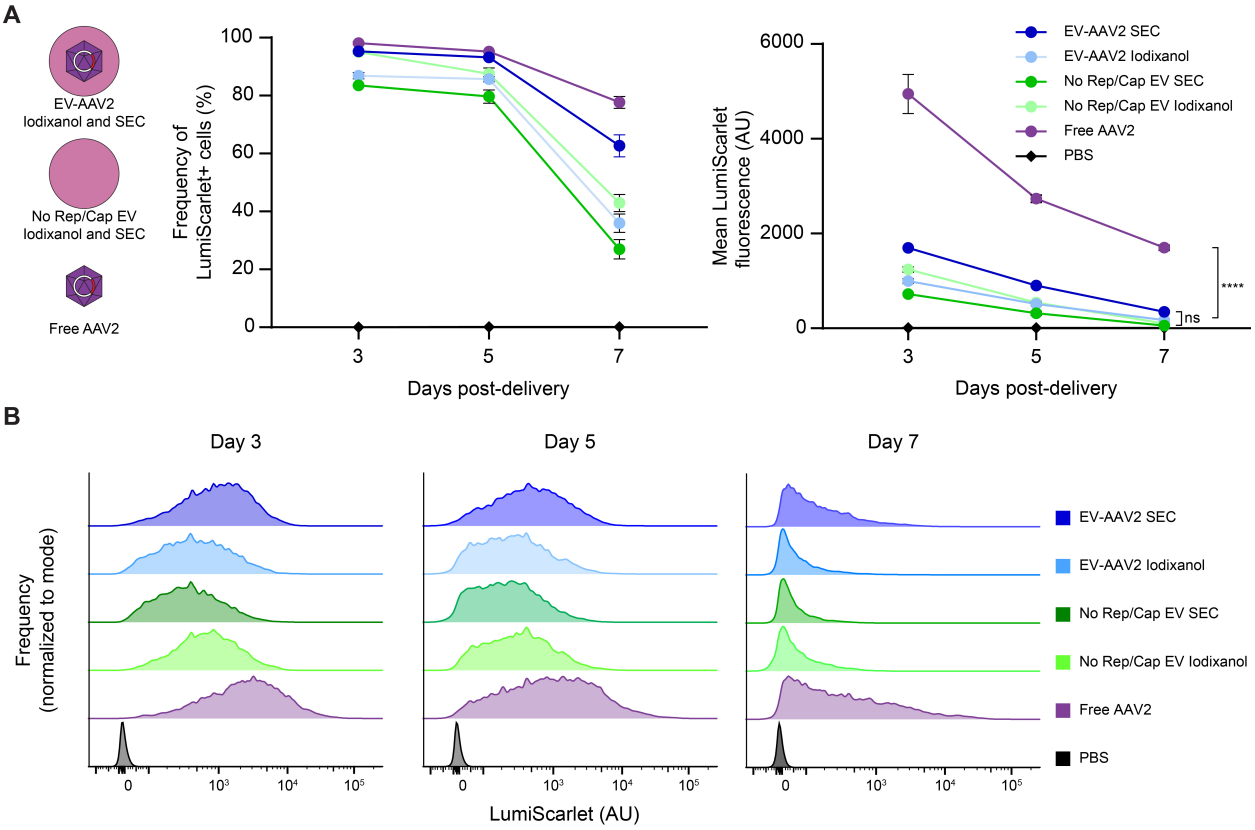

881

882 Figure 1

883

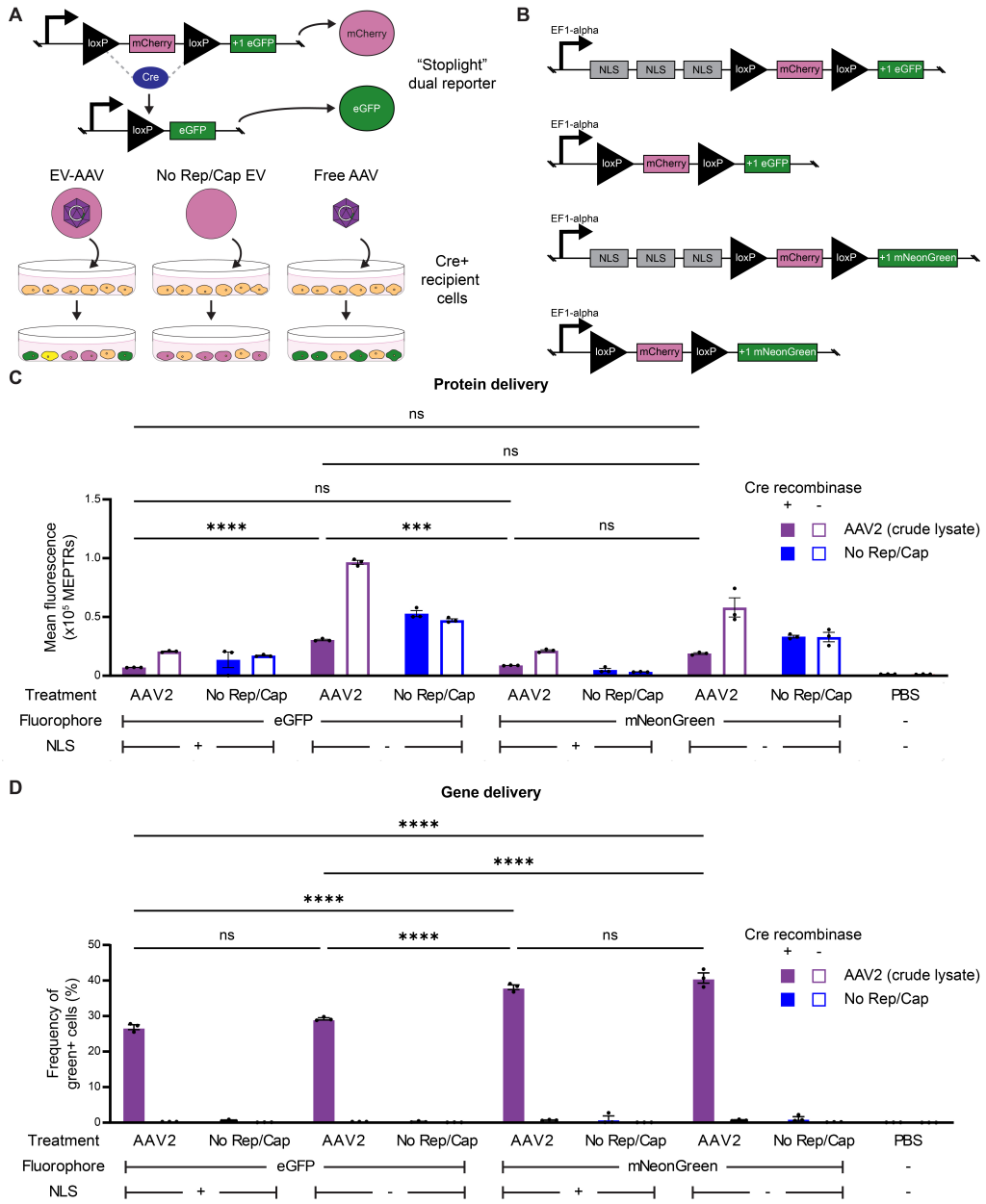
A
loxP
mCherry
loxP
+1 eGFP
mCherry
Cre
eGFP
loxP
eGFP
"Stoplight" dual reporter
EV-AAV
No Rep/Cap EV
Free AAV
Cre+ recipient cells
B
EF1-alpha
NLS
NLS
NLS
loxP
mCherry
loxP
+1 eGFP
+1 mNeonGreen
C
Protein delivery
ns
****
***
Cre recombinase
+
-
AAV2 (crude lysate)
No Rep/Cap
Mean fluorescence (x10^5 MEPTRs)
1.5
1.0
0.5
0
Treatment
AAV2
No Rep/Cap
PBS
Fluorophore
eGFP
mNeonGreen
NLS
D
Gene delivery
****
ns
Frequency of green+ cells (%)
50
40
30
20
10
0

Figure 2

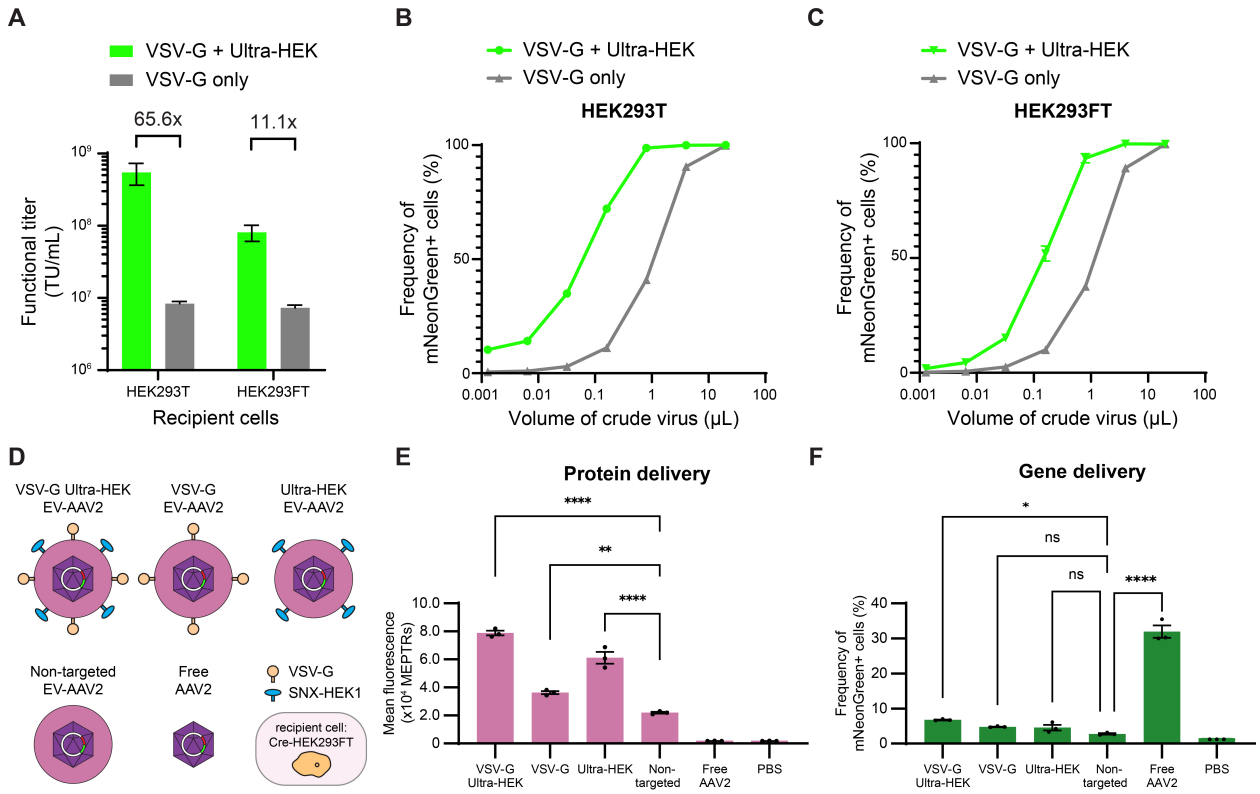
A
VSV-G + Ultra-HEK
VSV-G only
65.6x
11.1x
Functional titer (TU/mL)
HEK293T
HEK293FT
Recipient cells
B
VSV-G + Ultra-HEK
VSV-G only
HEK293T
Frequency of mNeonGreen+ cells (%)
Volume of crude virus (µL)
C
VSV-G + Ultra-HEK
VSV-G only
HEK293FT
Frequency of mNeonGreen+ cells (%)
Volume of crude virus (µL)
D
VSV-G Ultra-HEK EV-AAV2
VSV-G EV-AAV2
Ultra-HEK EV-AAV2
Non-targeted EV-AAV2
Free AAV2
VSV-G
SNX-HEK1
recipient cell: Cre-HEK293FT
E
Protein delivery
Mean fluorescence (x10⁴ MEPTRs)
VSV-G Ultra-HEK
VSV-G
Ultra-HEK
Non-targeted
Free AAV2
PBS
F
Gene delivery
Frequency of mNeonGreen+ cells (%)
VSV-G Ultra-HEK
VSV-G
Ultra-HEK
Non-targeted
Free AAV2
PBS

Figure 3

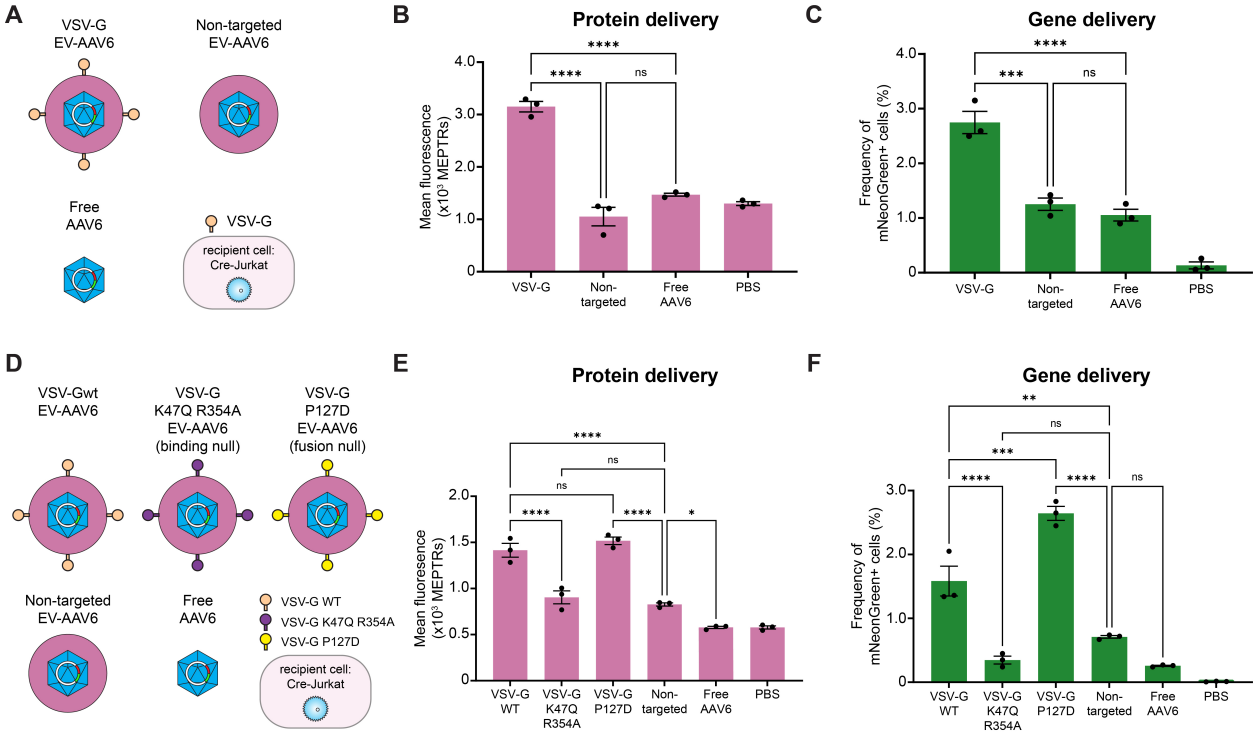

Figure 4

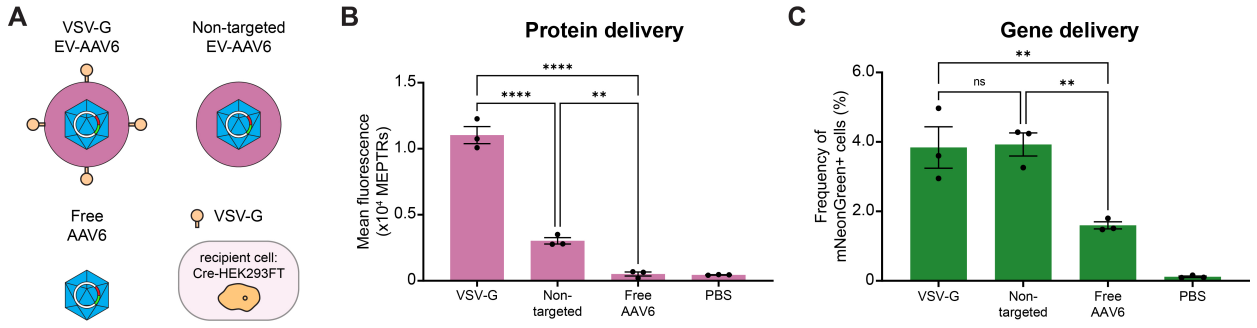

Figure 5

897 **FIGURE CAPTIONS**

898 **Figure 1: EV-AAV pseudotransduction complicates distinguishing protein delivery from gene**
899 **delivery. (A)** EV-AAV-mediated protein delivery and/or expression in HEK293FT recipient cells. Vector
900 compositions and EV-AAV purification methods employed to separate EVs and free AAV are summarized
901 in cartoons at left. Free AAV (which should confer minimal protein delivery) conferred significantly greater
902 fluorescence than did EV-AAV controls. EV-AAV vectors were generally similar to the No Rep/Cap (protein
903 delivery only) control at all time points post-delivery. **(B)** Representative histograms of LumiScarlet
904 fluorescence from samples reported in (A). No subpopulations are apparent than can rigorously distinguish
905 protein delivery from gene delivery. Experiments were performed in biological triplicate. Data shown are
906 from one of two independent experiments. Error bars indicate standard error of the mean. Multicomparison
907 statistical analysis was performed using a two-way ANOVA test, followed by Tukey's multiple comparison
908 test to evaluate specific comparisons (****$p < 0.0001$). ns; not significant; PBS: phosphate-buffered saline;
909 SEC: size exclusion chromatography.

910

911 **Figure 2: A Cre recombinase-based dual reporter system distinguishes protein delivery and gene**
912 **delivery. (A)** Schematic depicting the expected function of the stoplight dual-reporter system in which Cre
913 expressed in recipient cells acts upon incoming AAV genomes to switch them from expression of a red
914 reporter to a green reporter. Free AAV mediates gene delivery only (green); EV-AAV mediates both protein
915 delivery (red) and gene delivery (green) and sometimes both (yellow); No Rep/Cap EVs can only mediate
916 protein delivery (red). **(B)** Cre-responsive plasmids evaluated in this experiment. **(C,D)** Protein delivery (C)
917 and gene delivery (D) conferred by various vector compositions. Note: some mCherry gene expression
918 could occur in recipient cells prior to Cre-mediated recombination (or in the possible absence of
919 recombination in some cells), such that (C) includes both protein delivery and this ambiguous de novo gene
920 expression. Samples were normalized to include 1e9 vector genomes (for AAV crude lysate conditions) or
921 a volume-equivalent of the AAV2 crude lysate condition for No Rep/Cap crude lysate conditions (10^4
922 recipient cells). Experiments were performed in biological triplicate. Data shown are from one of two
923 independent experiments. Error bars indicate standard error of the mean. Multicomparison statistical
924 analysis was performed using a two-way ANOVA test, followed by Tukey's multiple comparison test to

925 evaluate specific comparisons (*$p < 0.05$, **$p < 0.01$, ***$p < 0.001$, ****$p < 0.0001$). NLS: nuclear
926 localization sequence; ns: not significant; PBS: phosphate-buffered saline.
927
928 **Figure 3: EV-AAV2 functionalization increases protein delivery but not gene delivery to HEK293FTs.**
929 **(A-C)** Validation of Ultra-HEK (Syenex) for enhancing lentiviral delivery to HEK293T and HEK293FT cells.
930 Relative fold-improvements in functional titer compared to a standard VSV-G-pseudotyped lentiviral vector
931 are indicated (**D**) Schematic depicting vectors used in (E,F) (Cre-HEK293FT recipient cells). (**E,F**) Protein
932 (E) and gene (F) delivery to HEK293FT cells (5 days post-delivery). Samples were normalized to include
933 1e9 vector genomes per condition (10^4 recipient cells). VSV-G and Ultra-HEK-functionalized EV-AAV
934 increase protein delivery but only modestly increase gene delivery and only when combined. Experiments
935 were performed in biological triplicate. Data shown are from one of two independent experiments. Error
936 bars indicate standard error of the mean. Multicomparison statistical analysis was performed using a one-
937 way ANOVA test, followed by Tukey's multiple comparison test to evaluate specific comparisons (*$p < 0.05$,
938 **$p < 0.01$, ***$p < 0.001$, ****$p < 0.0001$). PBS: phosphate-buffered saline.
939
940 **Figure 4: VSV-G functionalization of EV-AAV6 increases gene and protein delivery to Jurkat T cells**
941 **by increasing uptake. (A)** Schematic depicting vectors used in (B,C) (Cre-Jurkat T cell recipient cells).
942 (**B,C**) Protein (B) and gene (C) delivery to Jurkat T cells (5 days post-delivery). Samples were normalized
943 to include 1e9 vector genomes per condition (10^4 recipient cells). VSV-G functionalization significantly
944 increases protein delivery and gene delivery to Jurkats. **(D)** Schematic depicting vectors used in (E,F) (Cre-
945 Jurkat T cell recipient cells). (**E,F**) Protein (E) and gene (F) delivery to Jurkat T cells (5 days post-delivery).
946 Samples were normalized to include 2e9 vector genomes per condition (10^4 recipient cells). VSV-G
947 functionalization significantly increases protein delivery and gene delivery to Jurkats. Protein delivery and
948 gene delivery is increased only by enhanced binding of recipient cells (VSV-G WT and VSV-G P127D
949 vectors). Experiments were performed in biological triplicate. Data shown are from one of two independent
950 experiments. Error bars indicate standard error of the mean. Multicomparison statistical analysis was
951 performed using a one-way ANOVA test, followed by Tukey's multiple comparison test to evaluate specific
952 comparisons (*$p < 0.05$, **$p < 0.01$, ***$p < 0.001$, ****$p < 0.0001$). PBS: phosphate-buffered saline.

953

954 **Figure 5: Determinants of EV-AAV delivery to HEK293FT cells apply across AAV serotypes. (A)**
955 Schematic depicting vectors used in (B,C) (Cre-HEK293FT recipient cells). (**B,C**) Protein (B) and gene (C)
956 delivery to HEK29FT cells (5 days post-delivery). Samples were normalized to include 1e9 vector genomes
957 per condition (10^4 recipient cells). VSV-G functionalization enhances protein delivery by not gene delivery
958 by EV-AAV6, concordant with observations made using EV-AAV2. Experiments were performed in
959 biological triplicate. Data shown are from one of two independent experiments. Error bars indicate standard
960 error of the mean. Multicomparison statistical analysis was performed using a one-way ANOVA test,
961 followed by Tukey's multiple comparison test to evaluate specific comparisons (*$p < 0.05$, **$p < 0.01$,
962 ***$p < 0.001$, ****$p < 0.0001$). PBS: phosphate-buffered saline.

963